Glass transition-related thermorheological complexity in polystyrene melts

2007 J. Phys.: Condens. Matter 19 466101

(http://iopscience.iop.org/0953-8984/19/46/466101)

IOP PUBLISHING JOURNAL OF PHYSICS: CONDENSED MATTER

J. Phys.: Condens. Matter **19** (2007) 466101 (31pp) doi:10.1088/0953-8984/19/46/466101

Glass transition-related thermorheological complexity in polystyrene melts

Y-H Lin

Department of Applied Chemistry, National Chiao Tung University, Hsinchu, Taiwan

E-mail: yhlin@mail.nctu.edu.tw

Received 28 June 2007, in final form 12 September 2007
Published 10 October 2007
Online at stacks.iop.org/JPhysCM/19/466101

Abstract

The relaxation-modulus $G(t)$ functional forms covering the whole time range are given by incorporating a stretched exponential for the structural- (glassy-) relaxation process into the extended reptation theory (ERT; for entangled systems) or the Rouse theory (for entanglement-free systems). The creep compliance $J(t)$ curves of two entangled (A and B) and one entanglement-free (C) polystyrene samples (Plazek) as well as the viscoelastic spectra $G^*(\omega)$ of four entanglement-free polystyrene samples (Inoue *et al*) have been quantitatively analyzed in terms of the given $G(t)$ functional forms. In such quantitatively successful analyses, the ERT or the Rouse theory works as the frame of reference in both the line shape and timescale. The thermorheological complexity in the $J(t)$ curves is explained naturally and precisely by the temperature dependence of the *energetic-interaction-derived* structural relaxation being stronger than that of the *entropic* ERT or Rouse dynamics in a simple way. Structural-relaxation times $\tau_S(=18s'K')$ of all the studied samples are equally well separated into two decoupled quantities: the structural-growth parameter s' and the frictional factor K' (for the Rouse–Mooney or Rouse modes of motion). The separation is fundamentally a clean-cut process: s' is determined entirely by the *line shape* of $J(t)$ or $G^*(\omega)$ while K' is calculated from the timescale *shifting factor* obtained from the superposition of the calculated curves onto the measured. The glassy-relaxation strength A_G^f and the stretching parameter β extracted from the $J(t)$ and $G^*(\omega)$ results over the glassy-relaxation region are in good agreement. The glass-transition temperature T_g is defined as corresponding to $\tau_S = 1000$ s for all the studied samples. The τ_S, s' and K' data points of samples A, B and C extracted from their $J(t)$ curves individually fall closely on the same curves when expressed as a function of $\Delta T = T - T_g$, revealing a T_g-related universality within the polystyrene system, entangled or not. The revealed universality confirms the previously derived conclusion that the ERT and the Rouse theory have the same footing at the Rouse-segmental level. Representing important physical features of the universality, the length-scale of the structural relaxation

increases as ΔT diminishes and reaches the value of ∼3 nm at $\Delta T = 0$ (or at T_g) for all three samples, A, B and C. Extracted from the $G^*(\omega)$ results, the τ_S, s' and K' data of samples with molecular weights just below and well below entanglement molecular weight M_e (13 500) are found to deviate more from the respective universal curves with decreasing molecular weight. Deviation is estimated to start occurring at $M_w = 12\,000$.

1. Introduction

In the study of polymer viscoelasticity, often one of the three viscoelastic responses, relaxation modulus $G(t)$, viscoelastic spectrum $G^*(\omega)$ or creep compliance $J(t)$, is chosen for measurement [1–3]. On the basis of Boltzmann's superposition principle [1–3], the three different viscoelastic responses are equivalent, containing the same static and dynamic information; one form can be converted into another by a mathematical transformation. In the comparison of an experimentally measured $J(t)$ or $G^*(\omega)$ with a theoretical $G(t)$ functional form, the numerical calculation of the transformation from $G(t)$ can be accurately carried out [4, 5].

About 40 years ago thermorheological complexity in polystyrene melts was first observed by Plazek as the temperature approaches the glass-transition temperature T_g [6, 7]. The effect can be easily noticed, as the change in the long-time region of the creep compliance $J(t)$ with temperature is weaker than that in the short-time region. As reported previously [4], the $J(t)$ curves of two entangled nearly monodisperse polystyrene samples A and B (table 1) over the whole range have been quantitatively analyzed with the extended reptation theory (ERT) [2, 4, 8–11] as the frame of reference. The vital basis for the ERT to serve as the reference frame is its Rouse-segmental frictional factor K being independent of molecular weight as expected from the theory (see table 1 of [4]). The molecular-weight independence of K has been shown from analyzing the relaxation-modulus $G(t)$ line shapes of a series of nearly monodisperse polystyrene samples quantitatively in terms of the ERT and calculations from the viscosity and diffusion data by means of the ERT [2, 4, 8–11] (see appendix B of [4]). As the logical consequence of K being independent of molecular weight, ERT explains the molecular-weight dependences of the zero-shear viscosity and steady-state compliance; and their respective transition points, M_c and M_c'. The quantitative validity of the ERT as indicated by these results is only applicable in nearly monodisperse systems [2, 8–14]; all the viscoelastic responses or properties studied or referred to in this paper are of systems satisfying this condition. The line shape in the large-compliance region of $J(t)$ is essentially determined entirely by the contribution from the ERT dynamic processes and its timescale is characterized by the frictional factor K. Thus, the temperature dependence of the glassy-relaxation timescale as contained in and extractable from the short-time region of $J(t)$ can be studied with respect to that of K. In the ERT (as well as in the Rouse theory [2, 15, 16]), the frictional factor K is defined by

$$K = \frac{\zeta \langle b^2 \rangle}{kT\pi^2 m^2}, \tag{1}$$

where ζ, $\langle b^2 \rangle$ and m are the frictional constant, mean square bond length and mass of the Rouse segment, respectively. The $G(t)$ functional form for the whole time range of an entangled system is given by incorporating a stretched exponential for the glassy-relaxation process into the ERT (see section 2). From the given $G(t)$, the $J(t)$ line shape can be calculated with K fixed at a certain value through the basic equation of linear viscoelasticity [1–4]:

$$t = \int_0^t J(t')G(t - t')\,\mathrm{d}t'. \tag{2}$$

Table 1. Characteristics, M_w, M_w/M_n and T_g (based on DSC, and defined at $\tau_S = 1000$ s), and parameters, A_G^f, β and Z, extracted from the analyses of creep-compliance curves $J(t)$ ([4] and present study) or viscoelastic spectra $G^*(\omega)$ (present study) of the samples whose structural-relaxation times τ_S, structural-growth parameters s' and frictional factors K' are displayed in figures 6–8, as well as the reference theories used in the analyses. Also shown are K values at 127.5 °C and M_w, M_w/M_n, T_g and K at 127.5 °C of F1.

Sample	M_w	Reference theory	$Z(M_w/M_n)$	T_g (°C) DSC[a]	T_g (°C) $\tau_S = 1000$ s	K (s Da^{-2}) (127.5 °C)	A_G^f ($\times 10^{10}$ dyn cm^{-2})	β	Displayed in figures 6–8
Sample A	46 900	ERT	20(1.05)	97	97	4.8×10^{-9}	1.295(100 °C)	0.41	τ_S, s', K' from $J(t)$
Sample B	122 000	ERT	20(1.05)	100	99.6[b]		0.973(100 °C)	0.41	τ_S, s', K' from $J(t)$
Sample C	16 400	Rouse	20(1.05)	93.4	93.8	4.15×10^{-9}	0.993(100 °C)	0.42	τ_S, s', K' from $J(t)$
L10	10 500	Rouse	50(1.02)	90	(90.03)[c]		0.993(105 °C)	0.42	τ_S, s', K' from $G^*(\omega)$
A5000	5 970	Rouse	50(1.02)	82	(81.64)[c]		1.09(100°C)	0.42	τ_S, s', K' from $G^*(\omega)$
A2500	2 630	Rouse	20(1.05)	(59.6)[d]	(59.43)[c]		1.09(80 °C)	0.42	τ_S, s', K' from $G^*(\omega)$
A1000	1 050		(1.13)	(5)[d]	6.22		1.14(25 °C)	0.36	τ_S from $G^*(\omega)$
F1	16 700	ERT	120(1.01)	93.5		4.0×10^{-9}			

[a] Values based on the DSC results shown in figure 3 of [38].
[b] 'Restored' to the uncontaminated state.
[c] Calculated by extrapolation from the FTH equation best fitted to the obtained τ_S values.
[d] Outside the molecular-weight range covered in figure 3 of [38]; thus, estimated from the T_g values determined by DSC as reported in [32] and adjusted by subtracting 3.8 °C which is the average difference between the two sets of DSC values.

The calculation can be accurately done numerically using the Hopkins–Hamming [4, 17, 18] method (see appendix A of [4]). Then the frictional factor K can be determined from the timescale shifting factor obtained in the superposition of the calculated $J(t)$ line shape on the measured curve. The K value obtained from the $J(t)$ of sample A this way is in close agreement with the previously obtained values (table 1 of [4]).

While being independent of molecular weight, K carries the temperature dependence—often described by the Fulcher–Tammann–Hesse (FTH) equation or the Williams–Landel–Ferry (WLF) equation [19–21]—of all the relaxation times of the processes in the rubber-to-fluid region. As opposed to the *entropic* nature of the dynamics in this region, the glassy-relaxation process that occurs in the short-time region is derived from the *energetic interactions* within and between segments. The temporally uneven thermorheological complexity in the $J(t)$ curves of sample A and sample B has been shown to arise from the temperature dependence in the energetic-interaction-derived dynamics being stronger than that of the entropy-derived dynamics in a simple way. The difference in temperature dependence can be characterized in terms of the parameter s defined by

$$s = \frac{\langle\tau\rangle_{\mathrm{G}}}{K}, \tag{3}$$

where $\langle\tau\rangle_{\mathrm{G}}$ is the average glassy-relaxation time. From the quantitative analyses of the $J(t)$ curves of sample A and sample B, it has been found that s increases by about an order of magnitude with decreasing temperature over a range of $\sim$20° just above T_{g}.

According to the successful analysis in terms of equation (3), the thermorheological complexity should occur in a polystyrene melt as long as its molecular weight is greater than that of a Rouse segment, which has been estimated to be 850 [22–30]. A scheme of analysis equivalent to that for the entangled systems (sample A and sample B) may be formed for analyzing an entanglement-free system by replacing the ERT with the Rouse theory as the frame of reference. In terms of such a $G(t)$ functional form the J_{e}^0 and $J(t)$ results of sample C [31] (A-61[3] of [31]) (table 1) and the $G^*(\omega)$ results of L10, A5000, A2500 and A1000 [32] (table 1) are analyzed in this study.

T_{g} is defined by the temperature at which the structural-relaxation time τ_{S} reaches 1000 s for all the samples. The thus defined T_{g} serving as the common reference point, the structural and dynamic quantities obtained from analyzing the $J(t)$ results of samples A, B and C as well as the $G^*(\omega)$ results of L10, A5000, A2500 and A1000 are compared. The fundamental relationships between viscoelasticity—particularly, the glassy relaxation—and the glass transition are revealed.

Because the comparison of the analysis-obtained results of both entangled and entanglement-free samples will be discussed in terms of the $G(t)$ functional forms used to analyze their experimental results, the $G(t)$ functional form for the entangled samples [4] will first be briefly reviewed. Then the $G(t)$ functional form for the entanglement-free system used to analyze the results of entanglement-free samples in this study will be introduced. In the process, the relations between the two, important for later discussions, will be pointed out.

2. $G(t)$ functional forms in the entanglement and entanglement-free regions

Incorporating the glassy-relaxation process into the ERT, the relaxation modulus $G(t)$ for a nearly monodisperse entangled sample is expressed as [4]

$$G(t) = \frac{4\rho RT}{5M_{\mathrm{e}}} F(t) \int f(M) G_{\mathrm{E}}(M, t)\, \mathrm{d}M, \tag{4}$$

with

$$G_{\mathrm{E}}(M,t) = [1 + \tfrac{1}{4}\mu_{\mathrm{X}}(t/\tau_{\mathrm{X}}(M))]\big[\sqrt{M_{\mathrm{e}}/M}\,\mu_{\mathrm{B}}(t/\tau_{\mathrm{B}}(M)) + (1 - \sqrt{M_{\mathrm{e}}/M})\mu_{\mathrm{C}}(t/\tau_{\mathrm{C}}(M))\big] \tag{5}$$

and

$$F(t) = 1 + \mu_{\mathrm{A}}(t/\tau_{\mathrm{A}}) + A_{\mathrm{G}}\mu_{\mathrm{G}}(t/\tau_{\mathrm{G}}). \tag{6}$$

In equation (4), $f(M)$ is the molecular-weight distribution of the sample under study, $\mu_{\mathrm{X}}(t)$ the chain slippage through entanglement links to equilibrate the uneven tension along the primitive chain, $\mu_{\mathrm{B}}(t)$ the primitive-chain contour-length fluctuation and $\mu_{\mathrm{C}}(t)$ the reptation motion corrected for the chain-length-fluctuation effect. In equation (6), $\mu_{\mathrm{G}}(t)$ represents the glassy relaxation and A_{G} is its relaxation strength, and $\mu_{\mathrm{A}}(t)$ represents the Rouse–Mooney normal modes of motion [2, 8, 33, 34] of an entanglement strand with both ends fixed. The relaxation times of the different processes in the ERT, $\mu_{\mathrm{A}}(t)$, $\mu_{\mathrm{X}}(t)$, $\mu_{\mathrm{B}}(t)$ and $\mu_{\mathrm{C}}(t)$, are each expressed as a product of the frictional factor K and a structural factor—a functional form containing M_{e} and/or M. We refer the functional forms of the four processes and their respective relaxation times to the previous publications [2, 4, 8–11] While the friction factor K in the three processes, $\mu_{\mathrm{X}}(t)$, $\mu_{\mathrm{B}}(t)$ and $\mu_{\mathrm{C}}(t)$, is independent of molecular weight as mentioned above, the frictional factor in the Rouse–Mooney process $\mu_{\mathrm{A}}(t)$, denoted by K', has been found to be greater than K by a factor R_K that depends on the normalized molecular weight M/M_{e} (equation (12)) [2, 9, 11]. As it turns out, the predetermined $R_K(M/M_{\mathrm{e}})$ factor plays a very important role in the T_{g}-related *universality* as revealed in this study. The relevance of $R_K(M/M_{\mathrm{e}})$, which represents the dynamic anisotropy existing in entangled systems, is discussed in detail in section 5.

It has been found that the glassy relaxation is well described by the stretched exponential or the Kohlrausch, Williams and Watts (KWW) equation:

$$\mu_{\mathrm{G}}(t/\tau_{\mathrm{G}}) = \exp(-(t/\tau_{\mathrm{G}})^{\beta}); \qquad 0 < \beta \leqslant 1. \tag{7}$$

With $\langle\tau\rangle_{\mathrm{G}} = \int_0^\infty \mu_{\mathrm{G}}(t)\,\mathrm{d}t$, equation (3) has been used to characterize the glassy-relaxation time as a function of temperature relative to the relaxation times in the $\mu_{\mathrm{A}}(t)$–$\mu_{\mathrm{X}}(t)$–$\mu_{\mathrm{B}}(t)$–$\mu_{\mathrm{C}}(t)$ region, which are all proportional to the frictional factor K—including $K' = R_K(M/M_{\mathrm{e}})K$ in $\mu_{\mathrm{A}}(t)$. The combination of equations (3)–(7) has been used to analyze the $J(t)$ results of sample A and sample B at different temperatures consistently and quantitatively [4, 5].

The Rouse theory quantitatively describes the viscoelastic responses of entanglement-free systems over the entropy region [2, 10, 35]. From the extensive studies of the blend solutions [2, 11], it has been shown that the frictional factor K in the ERT is the same as that in the Rouse theory within a small possible experimental error (<20%). In other words, the two theories have the same footing at the Rouse-segmental level. As pointed out above, thermorheological complexity should occur in a polystyrene melt as long as its molecular weight is greater than that of a Rouse segment. Thus, corresponding to equations (4)–(6) for a nearly monodisperse entangled polymer melt, the relaxation modulus for an entanglement-free melt is expressed by

$$G(t) = A_{\mathrm{G}}^{\mathrm{f}}\mu_{\mathrm{G}}(t) + \rho RT \int \frac{f(M)}{M}\mu_{\mathrm{R}}(t,M)\,\mathrm{d}M. \tag{8}$$

In equation (8), $A_{\mathrm{G}}^{\mathrm{f}}$ is the full relaxation strength of the glassy relaxation and is related to A_{G} of equation (6) by $A_{\mathrm{G}}^{\mathrm{f}} = A_{\mathrm{G}}\rho RT/M_{\mathrm{e}} = (5/4)A_{\mathrm{G}}G_N$.[1] Moreover, $\mu_{\mathrm{R}}(t,M)$ representing the

[1] Incorporating $A_{\mathrm{G}}\mu_{\mathrm{G}}(t)$ into the ERT or $A_{\mathrm{G}}^{\mathrm{f}}\mu_{\mathrm{G}}(t)$ into the Rouse theory is intended to be a phenomenological description. As the relaxation times of $\mu_{\mathrm{X}}(t)$, $\mu_{\mathrm{B}}(t)$ and $\mu_{\mathrm{C}}(t)$ are all much longer than the slowest in $\mu_{\mathrm{G}}(t)$, it makes no practical difference to express the glassy relaxation either as the $A_{\mathrm{G}}\mu_{\mathrm{G}}(t)$ term inside $F(t)$ (equation (6)) or as a separate term $A_{\mathrm{G}}^{\mathrm{f}}\mu_{\mathrm{G}}(t)$ in equation (8).

Rouse relaxation for the component with molecular weight M is given by

$$\mu_R(t, M) = \sum_{p=1}^{N-1} \exp\left(-\frac{t}{\tau_p}\right), \tag{9}$$

with

$$N = \text{cint}(M/m) + 1 \tag{10}$$

and

$$\tau_p = \frac{\zeta \langle b^2 \rangle}{24kT \sin^2(p\pi/2N)} = \frac{K\pi^2 M^2}{24N^2 \sin^2(p\pi/2N)}, \tag{11}$$

where the function cint(x) converts a number x to an integer by rounding the fractional part of x.

3. Analyses of the J_e^0 and $J(t)$ results

As shown previously [2, 4, 8–11, 35], $f(M)$ for a nearly monodisperse polystyrene sample as appearing in equation (4) or (8) is well represented by the Schulz distribution [36, 37] characterized by the polydispersity parameter $Z(M_w/M_n = (Z+1)/Z)$. The Z value of a studied system is determined as an adjustable parameter giving the best fitting to the line shape of the measured viscoelastic response. The quantitative line-shape analyses have all been warranted by the obtained Z values being well within the range expected for a nearly monodisperse sample [2, 4, 8–11, 35]. The analyses of the $J(t)$ results of samples A and B have been reported in detail in [4]; the J_e^0 and $J(t)$ results of sample C are analyzed as described in the following.

Based on sample C having a molecular weight just slightly above the entanglement molecular weight $M_e = 13\,500$ and a molecular-weight distribution that is not extremely narrow, it is not all clear whether it is an entangled or entanglement-free system. For achieving quantitative agreements between the calculated and measured results of both J_e^0 and $J(t)$ of sample C, the following factors need to be evaluated and determined. (1) The choice of the functional form—i.e. equation (4) or (8) or even a linear combination of equations (4) and (8) if the system behaves as an entangled blend solution [2, 11]. (2) The Z parameter for the molecular weight distribution $f(M)$. (3) The A_G (or A_G^f) and β values for the glassy-relaxation process. They can be best found by a trial-and-error process until consistently quantitative agreements are obtained. The functional form chosen must be well justified and consistent with the obtained Z parameter. Section 3.4 of [4] has been entirely devoted to the discussion of the technical sensitivities, uniqueness and physical meanings of the involved parameters or fitting parameters as well as their predeterminations or determinations for an entangled system. In particular, figure 3 of [4] illustrates how the calculated $J(t)$ line shape is affected by change in β. In the entanglement-free system, the number of parameters is reduced, as the ratio K'/K and the entanglement molecular weight M_e are not involved. As far as the glassy-relaxation process is concerned, the involved fitting parameters in the entangled and entanglement-free systems are the same. Thus, the discussion given in [4] is equally applied to the entanglement-free case.

For sample C, we have found that the combination of equation (8) and $Z = 20$ gives the best result. The uses of equation (8) and $Z = 20$ are closely related. In view of sample C's M_w value being above M_e, equation (4) instead of equation (8) should be used. However, sample C's molecular-weight distribution, though nearly monodisperse, is broad enough to have a sufficient total number of components with molecular weights below M_e, rendering the system entanglement free by dilution. At $Z = 20$ ($M_w/M_n = 1.05$), sample C has

21 wt% ($W_2 = 0.79$) of the distribution with molecular weights below M_e. The dilution increases the entanglement molecular weight from M_e to $M'_e = 17\,090$ as calculated from $M'_e = M_e/W_2$ [2, 11]. As $M'_e > M_w$, sample C immerses in an entanglement-free state. As opposed to such a situation, the viscoelastic responses, $G(t)$ and $G^*(\omega)$, of an extremely narrow polystyrene sample (F1) [2, 9, 10] with nearly the same M_w clearly could not be described by the Rouse theory. Instead, they were successfully analyzed in terms of the ERT with $Z = 120$ ($M_w/M_n < 1.01$) and $K'/K = 1$. In table 1, the results of sample F1 from the previous study are also listed for a later discussion.

With the explanation as given above, we shall use equation (8) as the chosen functional form in discussing the analyses of the J^0_e and $J(t)$ results of sample C below. With $\langle\tau\rangle_G$ being related to K by equation (3), an increase in s reducing the width of the relaxation-time distribution will lead to a decrease in J^0_e [2]. Thus, a computer program can be set up to scan through a wide range of s to calculate a large set of J^0_e values, from which the matching with the values determined experimentally at different temperatures can be identified.

The A^f_G and β values listed in table 1 for sample C allow consistent and quantitative matching of the calculated results with the $J(t)$ line shapes from 93 to 119.4 °C and the J^0_e values from 93 to 134.1 °C as obtained by Plazek [31]. The A^f_G and β values are, respectively, very much uniquely dictated by the compliance values and line shapes of $J(t)$ at 93 and 96 °C—namely, the short-time region of $J(t)$ [4].

We use 100 °C as the reference temperature at which the calculated and measured J^0_e values are matched. Thus, the experimental J^0_e values listed in table II of [31] are first adjusted by the multiplication factor $\rho T/\rho_0 T_0$ where ρ_0 is the density at $T_0 = 373$ K; the adjusted J^0_e will be denoted by J^0_{ep}. With the A^f_G and β values as chosen, from matching the calculated J^0_{ep} values with the adjusted experimental values, the s values at different temperatures are determined. These s values are then used to calculate the $J(t)$ line shapes for comparison with the measured curves. In general, the agreement between the thus calculated and the measured $J(t)$ is very close. The matching of the calculated with the measured $J(t)$ curves has been carried out with the aid of graphic software as done in [4].

The s values obtained from matching the calculated J^0_{ep} values with the measured ones have been modified slightly in some cases to obtain a better agreement between the calculated and measured $J(t)$ line shapes as shown in figure 1. The experimental $J(t)$ results shown in figure 1 are those shown in figure 1 of [31], which have all been reduced to using 100 °C as the reference temperature for the compliance—i.e. multiplied by $\rho T/\rho_0 T_0$. Accordingly, all the theoretical $J(t)$ curves are calculated at $\rho T/\rho_0 T_0 = 1$. Following Plazek's notation [31], the thus calculated $J(t)$ is denoted by $J_p(t)$; as used above and will be used below, the corresponding viscoelastic quantities $G(t)$, J^0_e and η will be denoted by $G_p(t)$, J^0_{ep} and η_p, respectively. In this study, each of the theoretical $J_p(t)$ curves is first calculated with $K = 10^{-4}$. In superposing the calculated on the measured $J_p(t)$ at a certain temperature, shifting only along the time axis is allowed. From each superposition, a timescale shifting factor, SF, is obtained, which, when multiplied by 10^{-4}, gives the K value at the corresponding temperature. Except for the results at 134.1 °C, s values obtained from fitting to the $J_p(t)$ line shapes and the corresponding SF and K values at different temperatures are listed in table 2. At 134.1 °C, due to the lack of the experimental $J_p(t)$ the s value obtained from matching the calculated and experimental J^0_{ep} values is listed in table 2. The K value at 134.1 °C has been determined in indirect ways using the viscosity enhancement factors at different temperatures that can be calculated from the s values as explained in the following.

Because the glassy relaxation occurs in the short-time region, its contribution to the zero-shear viscosity η_p, often referred to as the internal viscosity, is in general negligible if the molecular weight of the sample is sufficiently large. The contribution of the internal viscosity

Table 2. Structural and dynamic quantities extracted from the $J(t)$ line-shape analyses of sample C.

Temp. (°C)	$s' = s$ (Da^2)	SF	$K' = K$ (s Da^{-2})	$\log \eta_p$ ($K = 10^{-4}$)	$\eta_p/\eta_p(A_G = 0)$ ($K = 10^{-4}$)	$\rho T/\rho_0 T_0$	$\log \eta$ exp.	$\log \eta$ calc.	$\log J_e$ exp.	$\log J_e$ calc.	τ_S (s)
$A_G = 0$				10.159	1						
134.1	(1640)[a]		(1.06×10^{-9})	(10.205)	(1.111)	1.072	5.257	(5.261)	−6.75	(−6.75)	(3.13×10^{-5})
127.5			$[4.15 \times 10^{-9}]$[b]								$[1.28 \times 10^{-4}]$[b]
119.4	1800	3.09×10^{-4}	3.09×10^{-8}	10.210	1.125	1.042	6.730	6.717	−6.79	−6.75	1.00×10^{-3}
109.4	4400	6.89×10^{-3}	6.89×10^{-7}	10.275	1.306	1.021	8.116	8.122	−6.90	−6.87	5.46×10^{-2}
105.1	7000	3.6×10^{-2}	3.6×10^{-6}	10.331	1.486	1.012	8.882	8.893	−6.96	−6.98	4.54×10^{-1}
102.9	8990	8.33×10^{-2}	8.33×10^{-6}	10.370	1.626	1.008	9.270	9.294	−7.05	−7.05	1.35
100.6	13 200	0.245	2.45×10^{-5}	10.442	1.919	1.003	9.820	9.832	−7.16	−7.19	5.82
96	28 500	2.89	2.89×10^{-4}	10.633	2.979	0.993	11.088	11.090	−7.54	−7.57	1.48×10^{2}
93.7_{56}	[43 960][b]		$[1.19 \times 10^{-3}]$[b]								[1000][b]
93	52 300	20.8	2.08×10^{-3}	10.825	4.635	0.987	12.156	12.138	−7.94	−7.94	1.96×10^{3}

[a] The s value at 134.1 °C is determined from matching the calculated and experimental J^0_{ep} values. All the values inside parentheses at 134.1 °C are derived from using the thus determined s value; see the text.

[b] Calculated from the equations obtained from least-squares fittings to the values determined at different temperatures; see the text.

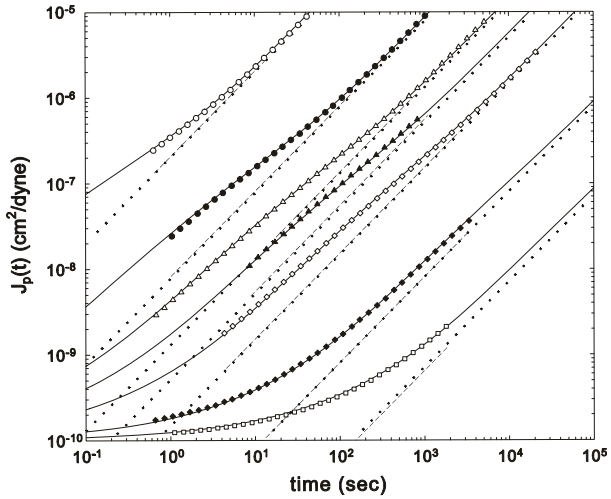

Figure 1. Creep compliance $J_p(t)$ data of sample C measured at 119.4 (○), 109.4 (●), 105.1 (△), 102.9 (▲), 100.6 (◇), 96 (◆), and 93 (□) °C in comparison with the theoretical curves (——; from left to right, respectively) calculated with the s and K values at different temperatures as listed in table 2; and the A_G^f and β values as explained in the text and given in table 1. Also shown is the comparison between the experimental (— — —) and calculated (+ + +) long-time $J_p(t)$ limits, t/η_p, at each corresponding temperature.

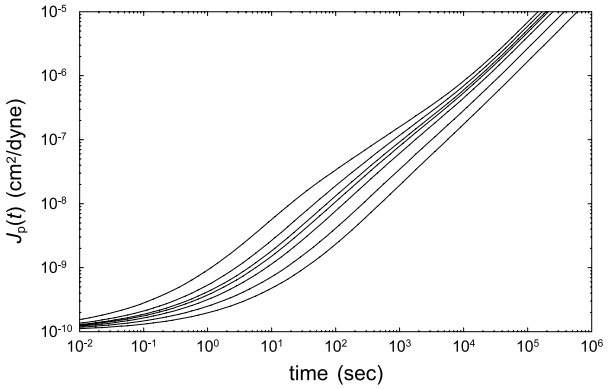

Figure 2. Comparison of creep compliance $J_p(t)$ curves of sample C calculated with $K = 10^{-4}$ and the s values (listed in table 2) corresponding to the calculated curves shown in figure 1; lines from left to right corresponding to 119.4, 109.4, 105.1, 102.9, 100.6, 96 and 93 °C, respectively.

to η_p in sample C is in general significant because of its relatively low molecular weight; thus, we may say that its viscosity is enhanced by the glassy-relaxation process. Using the obtained s values, including the one at 134.1 °C, the viscosity values containing the internal-viscosity contributions can be calculated, as listed under the $\eta_p(K = 10^{-4})$ column in table 2 with K set at 10^{-4}. Enhancements by the internal-viscosity contributions at different temperatures can be numerically evaluated by comparing the $\eta_p(K = 10^{-4})$ values with that calculated with the same K value but without the glassy-relaxation process (i.e., setting $A_G^f = 0$ in the calculation; see the first row of table 2). The enhancement by the internal viscosity is expressed as the ratio, $\eta_p(K = 10^{-4})/\eta_p(K = 10^{-4}; A_G^f = 0)$, as also listed in table 2. The contribution of the internal viscosity is only 11% at 134.1 °C and increases gradually more rapidly with decreasing

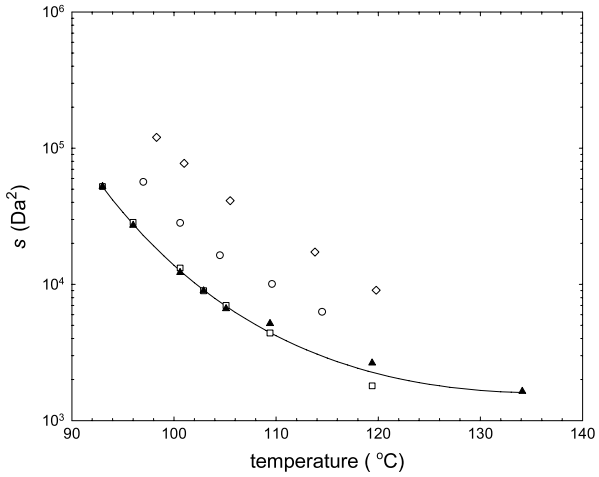

Figure 3. s values as a function of temperature of sample A (○), sample B (◇) and sample C (□ determined from the $J_p(t)$ line-shape analyses; ▲ from matching with the experimental J_{ep}^0 values; —— calculated from the modified FTH equation best fitting the data points).

temperature, enhancing the viscosity by a factor of 4.6 at 93 °C. As shown in figure 2, the large enhancement by the internal viscosity at a low temperature is reflected by the large shift of the corresponding $J_p(t)$ curve in the flow region to the longer *normalized* time (normalized on the basis of using $K = 10^{-4}$ for all the calculated curves) from one at a high temperature.

Dividing a measured viscosity value by both $\rho T/\rho_0 T_0$ and the viscosity enhancement factor $\eta_p(K = 10^{-4})/\eta_p(K = 10^{-4}; A_G^f = 0)$, a viscosity value, denoted by η_R, is obtained. The η_R value, as being free from the contribution of the internal viscosity and the small change in modulus with temperature, is linearly proportional to K. Then, the K value at 134.1 °C can be calculated from multiplying the K values at other temperatures by the ratios $\eta_R(134.1\,°C)/\eta_R(t\,°C)$. In this way, the average K value at 134.1 °C obtained from the K values at seven other temperatures is 1.06×10^{-9} with a standard deviation of only 3.5%. As any substantial error in s can cause a large error in the calculated η_R values, especially at low temperatures, the small standard deviation indicates that the s values are correctly obtained from the $J_p(t)$ line-shape analyses.

The two sets of s values as a function of temperature, obtained from the analyses of the J_{ep}^0 data and from analyzing of the $J_p(t)$ curves, are in good agreement (figure 3) indicating the consistency of the data analyses. The consistency is equivalently indicated by the close agreement between the experimental J_e^0 values and those calculated based on the s values obtained from the $J_p(t)$ line-shape analyses, as listed in table 2 and shown in figure 4. This agreement explains quantitatively the decline in J_e^0 of a low-molecular-weight sample with temperature decreasing towards T_g as due to the stronger temperature dependence of the glassy-relaxation process than that of the rubbery (entropy-derived) dynamics.

The K values shown in table 2 for sample C can be well fitted to an equation of FTH form. Using the FTH equation obtained from the fitting, the K values at 127.5 and 93.7_{56} °C are calculated and listed in table 2 for later use.

4. Analyses of the viscoelastic spectra $G^*(\omega)$

The $G^*(\omega)$ spectra of L10, A5000, and A2500 [32] are quantitatively analyzed in terms of equations (7)–(11) just as the $J(t)$ line shapes of sample C have been. The calculation of $G^*(\omega)$

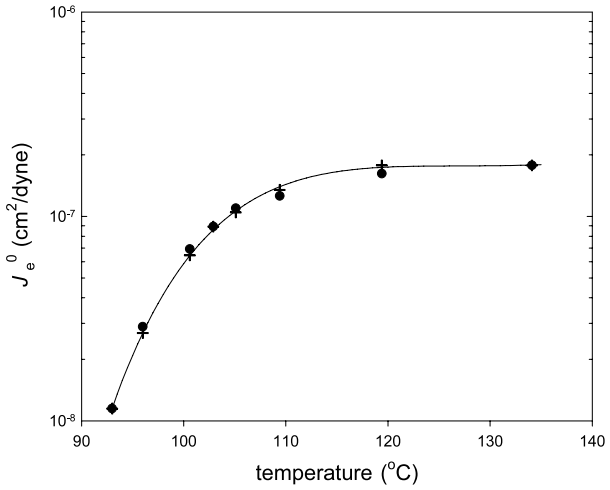

Figure 4. Comparison of the measured J_e^0 values (●) with those calculated (+) based on the s values obtained from the $J_p(t)$ line-shape analysis and the curve calculated from the empirical functional form $\log(J_e^0) = a + b/x + c/x^2 + d/x^3$ (x being the temperature in °C) best fitting the calculated values. Note: as the $J_p(t)$ curve at 134.1 °C is not available for analysis to obtain the s value, the J_e^0 value at 134.1 °C used in the least-squares fitting is the experimental value itself.

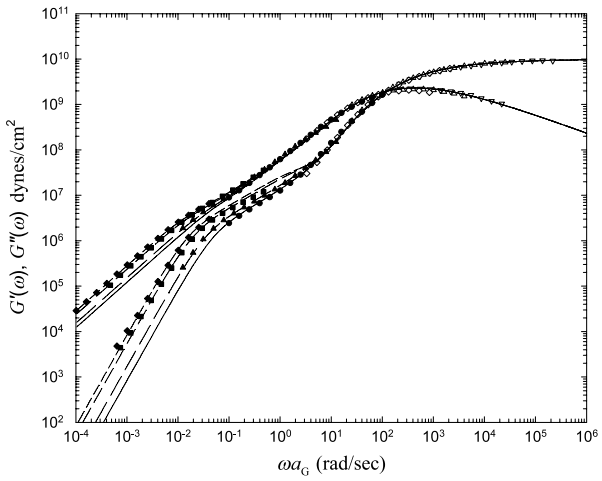

Figure 5. Comparison of the viscoelastic spectra $G^*(\omega)$ of L10 measured at different temperatures (▽ at 92 °C; △ at 95 °C; ◇ at 99 °C; ● at 105 °C; ▲ at 110 °C; ■ at 120 °C; ♦ at 130 °C) with the calculated (—— in the glassy-relaxation region; in the entropic region —— at 105 °C (ΔT = 15 °C); — — — at 110 °C (ΔT = 20 °C); – – – at 120 °C (ΔT = 30 °C); - - - - at 130 °C (ΔT = 40 °C)); the reference temperature is 105 °C (ΔT = 15 °C).

from a $G(t)$ functional form can be accurately done numerically according to the procedure described in the appendix of [5]. In the case of A1000, as the contribution of the Rouse modes of motion is negligible due to the molecular weight being very small—about that of a single Rouse segment $m = 850$—$G^*(\omega)$ is analyzed in terms of only a stretched exponential form for the glassy relaxation. The results of the $G^*(\omega)$ line-shape analyses are shown in figure 5 for L10. Those for samples A5000, A2500 and A1000 are shown in the appendix A.

In these figures, the spectrum at a certain temperature is chosen for each sample as the reference (for instance 105 °C for L10 as listed in table 1), onto which the line shapes of the

spectra measured at different temperatures are superposed over the glassy region to form a composite spectrum. From such a process, the timescale shift factors a_G with respect to the reference spectrum are obtained at different temperatures[2]. For each sample the average glassy-relaxation time at the reference temperature, $\langle\tau\rangle_G^0$, is determined from matching the calculated spectrum with the composite spectrum over the glassy-relaxation region. With the thus obtained $\langle\tau\rangle_G^0$ value, the $\langle\tau\rangle_G$ values at different temperatures are then calculated from the shift factors a_G for each sample. Simultaneously, the parameters A_G^f and β are extracted from fitting the calculated line shapes to the composite spectra over the glassy-relaxation region. As listed in table 1, the values of A_G^f and β obtained for L10, A5000 and A2500 are in good agreement with those of sample A, sample B and sample C. The M_w/M_n value of A1000 indicates that its molecular-weight distribution is broader than those of the other samples. With its small M_w value, A1000 should contain components with chain lengths as short as and shorter than the length-scale associated with the glassy-relaxation process in a polystyrene sample whose M_w value is not small. As a result, its glassy-relaxation time distribution is directly broadened by its molecular-weight distribution, leading to a β value smaller than for the other samples.

The $G^*(\omega)$ line shapes of samples L10, A5000 and A2500 in the entropic (or Rouse) region are affected by their molecular-weight distributions, though not in a sensitive way. It is sufficient to just use the Z values corresponding to the respective M_w/M_n values listed by Inoue *et al* [32] in the Schulz molecular-weight distributions without any further adjustment to calculate the $G^*(\omega)$ spectra. The close agreements between the calculated and measured spectra can be seen in figure 5 for L10. Similar close agreements are observed for A5000 and A2500 as shown in appendix A.

Just as in the cases of samples A, B and C, $\langle\tau\rangle_G$ (or structural-relaxation times τ_S; see equation (14)) of L10, A5000 and A2500 can be separated into two decoupled quantities: the structural-growth parameter s and the frictional factor K. As in the $J(t)$ line-shape analyses, s is entirely determined by the $G^*(\omega)$ line shape spanning over both the glassy-relaxation and entropic regions, while K is calculated from the timescale shifting factor. However, the way in which the $G^*(\omega)$ spectra at different temperatures are presented in figures 5 and A.1 is 'opposite to' that in which the $J(t)$ curves are presented in figures 1 and 2 of [4]. The $G^*(\omega)$ spectra are superposed onto one another over the glassy-relaxation region, while the $J(t)$ curves are composed together on the basis of using the same frictional factor K in calculating the theoretical curves. Thus, here the shifting factor a_G is first used to calculate $\langle\tau\rangle_G$ (or τ_S); then the frictional factor K is calculated from equation (3) using the s value determined from the line-shape analysis. By contrast, K as well as $K' = R_K(M/M_e)K$ is first calculated directly from the shifting factor in the analyses of the $J(t)$ curves.

5. Dynamic anisotropy in entangled systems

The K values obtained from analyzing the viscoelastic results at 127.5 °C of polystyrene samples of different molecular weights from 3.4×10^4 to 6×10^5 (table 1 and appendix B of [4])

[2] In the glassy-relaxation region, it may not be entirely proper to use the factor $\rho_0T_0/\rho T$, which is based on the theory of rubber elasticity to make small shifts along the modulus coordinate in forming the composite spectra. However, the largest temperature differences from the reference temperatures are no more than 25 °C and no superposition indicates a shift along the modulus coordinate is needed. Thus, the superposition of the spectra at different temperatures onto each reference spectrum is made by allowing shift only along the frequency axis. Technically, this is slightly different from the analyses of the creep compliance $J(t)$ and the steady-state compliance J_e^0, which have all been made on the results reduced along the compliance axis by the multiplication factor $\rho T/\rho_0T_0$ using 100 °C as the reference temperature. However, any discrepancies that may arise from this difference are expected to be negligibly small for the reasons as explained above.

in terms of the ERT have an average value of $4.9 \times 10^{-9} \pm 10\%$. As listed in table 1, the K value of F1 with $M_w = 1.24M_e$ is only about 20% below the average value [2, 9]. While these results of entangled systems indicate that the molecular-weight independence of K extends to a molecular weight virtually as low as just above M_e, T_g starts to decrease with decreasing molecular weight at around $10M_e$ [38, 39]. From the viewpoint of the conventional concept of the relation between viscoelastic dynamics and T_g as related to free volume [1, 40–45], this contrast represents a paradox. The paradox has been explained by the physical picture [2, 9, 11] that the free volume *at both chain ends* is always available to the modes of motion along the primitive path [46, 47] (namely the $\mu_X(t)$, $\mu_B(t)$ and $\mu_C(t)$ processes), whose relaxation times are all proportional to K. Such a mechanism may allow K to be disengaged from a dependence on the free volume *in the bulk* and become independent of molecular weight. Thus, it was proposed [2, 9, 11, 38] that the decrease in T_g with decreasing molecular weight in the entangled region should be related to the molecular-weight dependence of the K'/K ratio as described by the empirical equation

$$\frac{K'}{K} = R_K(M/M_e) = \frac{2.525}{\exp[-0.643((M/M_e) - 4.567)] + 1} + 0.769. \qquad (12)$$

As mentioned in section 2, K' is the frictional factor for the Rouse–Mooney process $\mu_A(t/\tau_A)$ (equation 9.B.20 of [2] or equation 20 of [8] with K replaced by K') in the ERT. $R_K(M/M_e)$ as given by equation (12) has been obtained from fitting the empirical functional form to the K'/K values obtained from the $G(t)$ line-shape analyses of a series of nearly monodisperse polystyrene samples [2, 9, 11] as mentioned. $R_K(M/M_e)$ has a plateau value of 3.3 in the high-molecular-weight region and starts to decline with decreasing molecular weight at around $M/M_e = 10$ to the limiting value of unity as $M/M_e \to 1$. $K'/K > 1$ indicates that the dynamics in an entangled system is anisotropic. $\mu_A(t/\tau_A)$ describes the motion of an entanglement strand with both ends fixed. Thus, unlike K being for the modes of motion along the primitive path that are always facilitated by the free volume at both chain ends, K' should be, like T_g, sensitive to the free volume in the bulk. Consistent with such a picture is the observation that T_g starts to decrease from its plateau value with decreasing molecular weight at around the same molecular weight ($M/M_e = 10$) as $R_K(M/M_e)$ does in the case of polystyrene [38, 39]. These results indicate that because of the tube (of the Doi–Edwards or reptation model [2, 46, 47]) the K value in the entanglement region is not affected by the decline in T_g with decreasing molecular weight. As far as polystyrene is concerned, equation (12) is part of the ERT used as the frame of reference for analyzing the $J(t)$ line shapes of sample A and sample B [4]. Furthermore, we shall see that normalizing (dividing) s by R_K unifies the analysis-obtained results of both entangled and entanglement-free polystyrene samples.

The need to normalize s by R_K is hinted at by the variations in s with temperature for samples A, B and C as shown together in figure 3. Very significantly, while different molecular theories are independently involved in the analyses for the entangled and entanglement-free systems, the s values of samples A, B and C change in a similar way in a similar range of temperature above their individual T_g values. Neglecting the small difference in T_g between sample A and sample B, it was pointed out [4] that their s values at the same temperature follow the molecular-weight dependence of K'/K, namely, $R_K(M/M_e)$ given by equation (12). This molecular-weight dependence of s is also borne out by the presentation of data in section 8 that has included sample C's results and taken the T_g dependence into account—T_g of sample C has decreased considerably due to its molecular weight being relatively small [38, 39]. s and K'/K having the same molecular-weight dependence as turned out should be closely related to the fact that the $\mu_G(t)$ and $\mu_A(t)$ processes are next to each other in timescale. To eliminate this

molecular-weight dependence in s, we define

$$s' = \frac{s}{(K'/K)} = \frac{\langle\tau\rangle_G}{K'} \tag{13}$$

in which equation (3) has been used for the second equality.

As reported previously [2, 9] and mentioned above, the quantitative analyses of the relaxation modulus and viscoelastic spectrum of F1 in terms of the ERT yielded $K'/K = 1$ within a small experimental error (<10%), indicating, as equation (12) does, $K'/K = 1$ as $M_w \to M_e$. When the tube is disappearing and the Rouse theory is becoming applicable at M_e, $K' = K$ is physically meaningful as it indicates that the dynamics in the system becomes isotropic as it should [2, 9, 11]. As the molecular weights of sample C and F1 are nearly the same and both very close to M_e, their K values are virtually the same (table 1). Thus, we may regard the s values of sample C as basically equivalent to that of F1 (with $K' = K$). Thus, we may have a pair of fictitious s' and K' defined as $s' = s$ and $K' = K$ for sample C (even though there is only one frictional factor in an entanglement-free system). As parts of the T_g-related universal behavior revealed in this study, the frictional factor K and the structural-growth parameter s in sample C play the same roles as K' and s', respectively, in the entangled systems sample A and sample B. In the presentations of the results, K and s of sample C are denoted by K' and s', respectively. Thus, whenever K' or s' of sample C is indicated below, automatically its K or s is meant or used. With this understanding, the notation $K' = K$ and $s' = s$ is also used in the entanglement-free cases with even smaller molecular weights: L10, A5000 and A2500, whose analysis-obtained results will be compared with those of sample A, sample B and sample C.

6. Comparison of the A_G^f and β values as extracted from $J(t)$ and $G^*(\omega)$ line shapes

The values of the glassy-relaxation strength A_G^f and stretching parameter β extracted from the $J(t)$ curves of sample A, sample B and sample C and those extracted from the $G^*(\omega)$ spectra of L10, A5000, A2500 and A1000 are listed together in table 1 for comparison. Because of the contamination by residual plasticizers, the somewhat smaller A_G^f value of sample B may be excluded from the comparison. Considering some differences in molecular weight and temperature, the agreement between the A_G^f and β values of sample A and sample C and those of L10, A5000 and A2500 is very good. As sample C and L10 have comparable molecular weights and the analyses of their results are made at temperatures very close to each other (100 versus 105 °C), the close agreement between them is particularly impressive. On the basis of Boltzmann's superposition principle [1–3], the agreement indicates the consistency between the $J(t)$ and $G^*(\omega)$ results in the glassy-relaxation region. In review of the special technical requirement for making accurate measurements of $J(t)$ of very low compliance or $G^*(\omega)$ of very high modulus in the glassy-relaxation region, such an agreement should be unusual to come by—the first of this kind to my knowledge. The agreement also signifies that the two sets of results from two independent laboratories [6, 7, 31, 32] support each other.

As $A_G^f = J(0)^{-1}$, the line shape of the glassy-relaxation process is mainly characterized by the stretching parameter β. The significance of the consistency between the β values obtained from the $J(t)$ and $G^*(\omega)$ line-shape analyses is much more than meets the eye—namely, much more than the consistency merely in the glassy-relaxation region—as explained in the following: the convolution integral (equation (2)) that converts $G(t)$ into $J(t)$ has the effect of smearing the separate processes in $G(t)$ and giving a much more featureless $J(t)$ line shape. The smearing effect has been clearly illustrated by the comparison of the $G(t)$ and $J(t)^{-1}$ curves calculated with and without the glassy-relaxation process included

as shown in figure 5 of [4]. By contrast, such a smearing effect basically does not exist in converting $G(t)$ into $G^*(\omega)$, as it is well known that the storage modulus spectrum $G'(\omega)$ is basically a mirror image of $G(t)$ if ω is regarded as $0.7t^{-1}$ [1, 5]. Thus, the analysis of the $J(t)$ line shape to extract the glassy-relaxation process is a much more challenging task than that of the $G^*(\omega)$ line shape. Without a correct functional form (either the ERT or the Rouse theory) for the entropic dynamic processes as the *base* (as the frame of reference), the glassy-relaxation process cannot be properly extracted from the $J(t)$ curve. As the ERT is being used for an entangled polystyrene system, the correctness includes the predetermined ratio $K'/K = R_K(M/M_e)$ as given by equation (12). Including this, we may summarize that the success of the ERT serving as the reference frame in the $J(t)$ line-shape analyses for the entangled polystyrene systems are testified to by the agreements between theory and experiment in three aspects: (1) the quantitative description of the $J(t)$ line shapes over the whole time range at different temperatures (figures 1 and 2 of [4]); (2) the frictional factor K obtained for sample A being in quantitative agreement with the values obtained previously and shown independent of molecular weight as expected from the theory (table 1 of [4]) and (3) the correctness of the predetermined $R_K(M/M_e)$ values for sample A and sample B as calculated from equation (12), which is strongly indicated by the obtained β values being consistent with those obtained for sample C, L10, A5000 and A2500 (table 1).

7. T_g defined by structural-relaxation time $\tau_S = 1000$ s

In [4], the structural- (or α-) relaxation time τ_S was defined by the time when the ratio between the contribution of the glassy-relaxation process (G) to the relaxation modulus $G(t)$ and that from all the entropic processes (R), G/R, reaches 3 [4, 5]. Physically, this means that G/R has decayed by a factor of e^{-1} from $G/R \sim 10$, which is the value at the relaxation time ($t = \tau_A^{15}$) of the highest Rouse mode when the temperature is at the glass-transition point. At the same time, the contribution from the glassy component in such a state is still significant. The structural-relaxation time defined this way is basically equivalent physically to that defined by [4, 5]

$$\tau_S = 18\langle\tau\rangle_G. \tag{14}$$

The structural-relaxation time as given by equation (14) has also been shown to be in close agreement with the α-relaxation time defined in a traditional way: the time at which the relaxation modulus reaches 10^8 dyn cm^{-2} (see figures 10 and 11) [1][3]. The structural-relaxation time defined by equation (14), besides reflecting the effect of the glassy relaxation on the bulk mechanical properties, has the virtue of following exactly the temperature dependence of the glassy-relaxation process. The other definitions are somewhat affected by the change in the line shape of the viscoelastic response with temperature—the thermorheological complexity.

Using equation (13), the structural-relaxation time given by equation (14) may be rewritten as

$$\tau_S = 18sK = 18s'K'. \tag{15}$$

From analyzing the $J(t)$ line shape of sample A at the calorimetric T_g (97 °C), it has been shown [4, 5] that the structural-relaxation time τ_S as defined by equation (15) reaches 1000 s with a corresponding length-scale of ∼3 nm, the order of magnitude as estimated by other methods [48–52]. In the literature [48, 53–55], τ_S reaching 100–1000 s has been used as the criterion for defining T_g. In view of the τ_S value for sample A at its calorimetric T_g, we shall use $\tau_S = 1000$ s for defining the T_g values of all other samples for the analyses and discussions

[3] See page 323 of [1] and reference 45 of [5]. The small difference between $G'(\omega) = 10^8$ dyn cm^{-2} and $G(t) = 0.8 \times 10^8$ dyn cm^{-2} is ignored here.

given below. It will be shown that the thus defined T_g values are consistent with the values expected from calorimetric measurements for all the studied samples (table 1). Including at the thus defined T_g, the dynamic and structural quantities at different temperatures, K, K', s' and τ_S, obtained from analyzing the $J(t)$ results of sample A [4, 5] are listed in table 3.

As sample B is contaminated by residual plasticizers [7], its frictional factor K is smaller than that of a normal sample as expected [4]. Because of the contamination, the T_g value of sample B has been estimated by Plazek to be smaller than that of a normal sample at the same molecular weight by about one degree [7]. The T_g of sample C is smaller than that of sample A because of its smaller molecular weight [38, 39]. Here we shall treat in a similar way the contamination by residual plasticizers in sample B causing its T_g to become smaller; in other words, we shall also use $\tau_S = 1000$ s to define the T_g of sample B *as it is*. From the s and K values extracted from the $J_p(t)$ of sample B available at the lowest temperature (98.3 °C), $\tau_S = 779$ s is obtained, which is a little smaller than the criterion $\tau_S = 1000$ s. Because the difference is not large, we may calculate the temperature at which $\tau_S = 1000$ s by extrapolation using the FTH equation that has been obtained from fitting to the τ_S values at different temperatures. The T_g determined this way for sample B is 98.0_{25} °C. Then from the FTH equation that best describes the K values of sample B at different temperatures, the K value at this temperature is obtained as listed in table 3. The s and s' values at T_g are then calculated from thus obtained τ_S and K values, using equation (15). The K, K' ($=3.16K$), s' and τ_S values of sample B at different temperatures [4] including those at T_g are listed in table 3.

By interpolation—using the FTH equation obtained from the least-squares fitting to the τ_S values listed in table 2—we obtained $\tau_S = 1000$ s at 93.7_{56} °C, which is then regarded as the T_g of sample C. Then, as also listed in table 2, the K' ($=K$) and s' ($=s$) values of sample C at this temperature can be obtained from their values at different temperatures by interpolation—using the FTH equation for K and a modified FTH equation (the form as given by equation (17)) for s.

The T_g values of L10, A5000, A2500 and A1000 as determined at $\tau_S = 1000$ s are described in appendix B. The T_g defined by $\tau_S = 1000$ s as explained above and in appendix B allows us to have a common *reference point* equivalent for the different samples, with respect to which we may compare the obtained τ_S, s' and K' results in perspective.

8. Dependences of τ_S, s' and K' on $\Delta T = T - T_g$

The analysis-obtained results of samples A, B and C strongly suggest that the τ_S and s' values of the three samples depend on how far the temperature is away from each individual T_g. Using the T_g defined by $\tau_S = 1000$ s for each sample (table 1), we display the τ_S values of samples A, B and C as a function of the temperature difference from T_g, $\Delta T = T - T_g$, in figure 6. In spite of the facts that sample C has a significantly smaller T_g due to its smaller molecular weight and that sample B is contaminated by residual plasticizers, the τ_S values of the three samples fall closely on the same curve. Note that both τ_S and T_g of sample B are determined for the sample as it is contaminated. Apparently, the contamination in sample B by plasticizers is so low that sample B has kept the T_g-related nature of polystyrene. The close agreement among the three samples strongly supports the method of using ΔT to account for the T_g difference. The τ_S values of the three samples can be collectively well fitted by the FTH equation of the form

$$\log(\tau_S) = a_\tau + \frac{b_\tau}{(\Delta T + t_\tau)} \tag{16}$$

as shown by the curve in figure 6 calculated with $a_\tau = -11.5045$, $b_\tau = 539.3497$ and $t_\tau = 37.1827$.

Table 3. Structural and dynamic quantities: s', K, K' and τ_S extracted from the $J(t)$ line-shape analyses of samples A and B.

Sample A					Sample B				
Temp (°C)	K (s Da^{-2})	$K' = 1.61K$ (s Da^{-2})	$s' = s/1.61$ (Da^2)	τ_S (s)	Temp (°C)	K (s Da^{-2})	$K' = 3.16K$ (s Da^{-2})	$s' = s/3.16$ (Da^2)	τ_S (s)
97	9.84×10^{-4}	1.58×10^{-3}	35 090	1000	[98.0_{25}][a]	[$4.40_3 \times 10^{-4}$]	[1.39×10^{-3}]	[39 930]	[1000]
100.6	9.7×10^{-5}	1.56×10^{-4}	17 560	49.4	98.3	3.6×10^{-4}	1.14×10^{-3}	38 060	779
104.5	1.2×10^{-5}	1.93×10^{-5}	10 150	3.53	101	6.02×10^{-5}	1.9×10^{-4}	24 500	83.9
109.6	1.2×10^{-6}	1.93×10^{-6}	6 244	0.217	103.3	1.52×10^{-5}	4.79×10^{-5}	18 640	16.1
114.5	1.96×10^{-7}	3.16×10^{-7}	3 903	0.0222	105.5	5.43×10^{-6}	1.72×10^{-5}	13 033	4.03
					113.8	1.49×10^{-7}	4.71×10^{-7}	5 474	4.64×10^{-2}
					119.8	2.61×10^{-8}	8.25×10^{-8}	2 867	4.26×10^{-3}

[a] Listed values at this temperature are calculated from the equations obtained from least-squares fittings to the values determined at different temperatures; see the text.

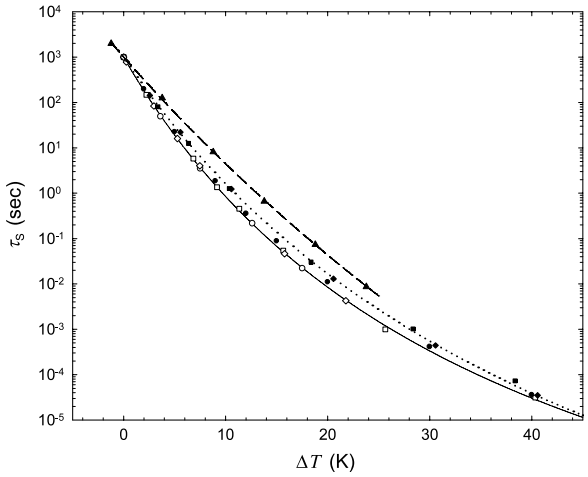

Figure 6. Structural-relaxation time, τ_S, values of sample A (○), sample B (◇) and sample C (□) as a function of the temperature difference from each individual T_g, ΔT. The solid line is calculated from the FTH equation (equation (16)) which best fits the data points of sample A, sample B and sample C collectively. Also shown are the τ_S data points of L10 (●), A5000 (■), A2500 (◆; with the best fitting FTH curve · · · · · ·) and A1000 (▲; with the best fitting FTH curve – – –) as a function of ΔT.

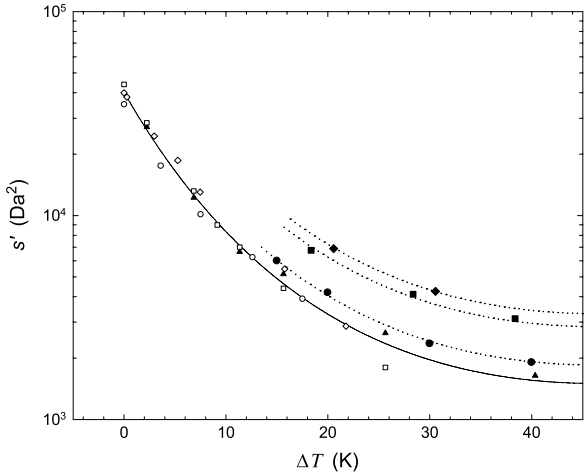

Figure 7. s' values of sample A (○), sample B (◇) and sample C (□ obtained from the $J_p(t)$ line-shape analysis; ▲ from matching the experimental J^0_{ep} values) as a function of the temperature difference from each individual T_g, ΔT. The solid line is calculated from the modified FTH equation (equation (17)) which best fits the data points of sample A, sample B and sample C collectively. Also shown are the s' data points of L10 (●), A5000 (■) and A2500 (◆) as a function of ΔT. The dotted lines each represent the universal curve multiplied by a factor to superpose on the data points of L10 (×1.23), A5000 (×1.9) and A2500 (×2.2) individually.

Shown in figure 7, the s' data points of samples A, B and C as a function of ΔT fall closely on the same curve. The ΔT dependence of s' of the three samples can be collectively well fitted by a modified FTH form:

$$\log(s') = c_1 + c_2(\Delta T + t_s) + \frac{c_3}{\Delta T + t_s}. \tag{17}$$

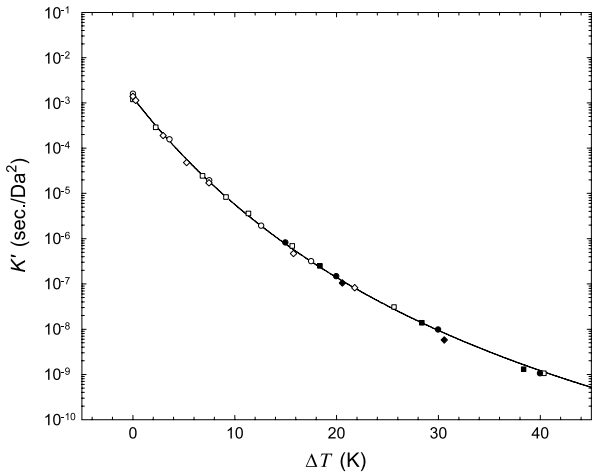

Figure 8. K' values of sample A (○), sample B (◇) and sample C (□) as a function of the temperature difference from each individual T_g, ΔT. The solid line is calculated from the FTH equation which best fits the data points of sample A, sample B and sample C collectively. Also shown are the K' data points of L10 (●), A5000 (■) and A2500 (♦) as a function of ΔT.

The curve shown in figure 7 has been calculated with $c_1 = -4.2189, c_2 = 0.0364, c_3 = 375.6136$ and $t_s = 55.0922$.

The consistency of the ΔT dependences of s' and τ_S individually falling on the same curves implies that the same consistency should occur for K' according to equation (15); indeed so as illustrated in figure 8. The ΔT dependences of K' of samples A, B and C can be collectively fitted by the FTH equation of the form given by equation (16) with the notations τ_S, a_τ, b_τ and t_τ replaced by K', a_K, b_K and t_K, respectively. The curve shown in figure 8 is calculated with $a_K = -15.3931, b_K = 536.9037$ and $t_K = 42.8976$. The K' values of samples A, B and C as a function of ΔT falling on the same curve indicates that the molecular-weight dependence of T_g is directly related to the molecular-weight dependence of K' as proposed previously [2, 9, 11, 38] and brought up in section 5. In the meantime, K is independent of molecular weight at and above 127.5 °C.[4] Therefore, as opposed to the consistency in the ΔT dependence of K' among samples A, B and C, their K values do not, as expected, have a common ΔT dependence.

8.1. T_g-related universality in polystyrene

It is remarkable that the τ_S, s' and K' data points of samples A, B and C as a function of ΔT individually fall *naturally* on the same curves as shown in figures 6–8, respectively. These results suggest a T_g-related universality. Although there are only three samples involved, such universality can indeed be claimed within the polystyrene system, because of the universal nature of the elements involved in the quantitative analyses of the $J(t)$ results of the three samples. These elements have been discussed in diverse parts of this report; it is advisable to summarize them briefly here.

[4] As shown in table 1 of [4], K is independent of molecular weight at 127.5 and 174 °C. It is also true that the temperature dependences of viscosity—reflecting the temperature dependence of K—at different molecular weights can be superposed on one another over the temperature range covered by viscosity measurements as reported in [31].

(1) The validity of the ERT and the universality it represents have been well tested previously [2, 4, 8–11]. The success of the ERT is further summarized in section 6 with the additional support obtained from this study. Indeed, as stated in section 3.4 of [4], 'Because of the success of ERT as represented by the molecular-weight independence of K, theoretically, there is no limit to the time range of $J(t)$ that can be analyzed, depending on the molecular weight of the sample under study'. On such a basis, the single quantitatively successful analysis case of sample A has all the ingredients for generalizing the success to polymers of other molecular weights. The results of sample B and sample C further support such a generalization.

(2) Sample B is contaminated by residual plasticizers; as a result, its obtained K value is appreciably smaller than the average value of normal samples as expected [4]. However, its K'/K ratio as can be calculated from equation (12), which represents the predetermined universal normalized molecular-weight dependence of K'/K in polystyrene, is not expected to be affected—both K' and K being affected by the same degree. The expected K'/K ratio of sample B is 3.16 and that of sample A is 1.61. As explained in section 5, one can regard sample C as having $K'/K = 1$—basically equivalent to substituting $M/M_e = 1$ into equation (12). These ratios are used to calculate s' and K' from s and K, respectively, of the three samples as explained in section 5. Thus, it is on the basis of being consistent with the universality of K'/K predetermined for polystyrene that the common curves of s' and K' shared by the three samples are obtained.

(3) The close agreements of the τ_S, s' and K' results of sample C as a function of $\Delta T = T - T_g$ with those of samples A and B should not be surprising even though two different molecular theories are independently involved. These close agreements actually should be expected on the basis of the previously derived conclusion that the ERT and the Rouse theory have the same basis at the Rouse segmental level [2, 11].

Finally, a comment should be made about the contamination by residual plasticizers in sample B. Its T_g value is determined by $\tau_S = 1000$ s of the sample as it is; concurrently, the obtained quantities τ_S, s' and K' are also associated with sample B as it is. Because the contamination is at a residual level, the T_g-related dynamic process of sample B is dominated by the characteristics of polystyrene. Thus, the results of τ_S, s' and K' as a function of $\Delta T = T - T_g$ of sample B as shown in figures 6–8 can be regarded as equivalent to those of a 'normal sample B'.

The three bases explained above enable the common curves of τ_S, s' and K' shared by samples A, B and C to be regarded as representing a T_g-related universality applicable within the polystyrene system, entangled or not. As shown below, the universality ends at around $M_w = 12\,000$, nearly 30% below the molecular weight of sample C.

From the above discussions, one may observe that the predetermined factor $R_K(M/M_e)$ plays a very important role interfacing this ΔT- or *T_g-related universality* occurring in the short-time region (the $\mu_G(t)$–$\mu_A(t)$ region) and the other *universality of topological nature*—topological constraint of entanglement—occurring in the long-time region (the $\mu_X(t)$–$\mu_B(t)$–$\mu_C(t)$ region). Putting it more specifically, on the one hand, the universal ΔT dependences of s' and K' cannot be obtained without $R_K(M/M_e)$; on the other hand, K' is converted by the factor $R_K(M/M_e)$ from K, which is independent of molecular weight at and above 127.5 °C (see footnote 4).

8.2. Deviation from the T_g-related universality

The obtained τ_S values for the four samples, L10, A5000, A2500 and A1000, are shown in figure 6 along with the results obtained for samples A, B and C. The τ_S results of L10, A5000 and A2500 shown in figure 6 indicate that deviation from the universal curve increases

gradually with decreasing molecular weight, moving towards the curve for A1000; the largest change occurs between A2500 and A1000. The data points of L10 cling closely to the universal curve, suggesting that the universality of the ΔT dependence of τ_S should extend to or end at a molecular weight between sample C and L10. The s' and K' values of L10 extracted from the $G^*(\omega)$ line-shape analyses are similarly close to or virtually on their respective universal curves as shown below.

The structural-growth parameter s' and the frictional factor K' for L10, A5000 and A2500 can only be extracted from a $G^*(\omega)$ spectrum that simultaneously spans both the glassy-relaxation and entropic regions. As the $G^*(\omega)$ spectra measured by Inoue *et al* [32] at low temperatures ($\Delta T < 14\,^\circ$C) cover only the glassy-relaxation region, the numbers of data points of s' and K' extractable from the spectra are considerably less than that of τ_S. As s' decreases with increasing temperature, the entropic region of the spectrum shifts further away from the glassy-relaxation region—K' increases with decreasing s' under the condition of τ_S being fixed, as $\tau_S = 18K's'$—as shown in figures 5 and A.1.

Shown in figures 7 and 8, respectively, are the obtained s' and K' values of L10, A5000 and A2500 in comparison with the results of samples A, B and C and the calculated universal curves. K' values of the low-molecular-weight samples are virtually on the universal curve, with slightly noticeable deviation towards the lower side only in the case of A2500. The success of using ΔT to account for the change in T_g with molecular weight is indeed extraordinary in the case of K', considering the large T_g drops of these samples from the plateau value, 100 °C (decreasing by 10, 18 and 40 °C in L10, A5000 and A2500, respectively [38, 39]; table 1). As $\tau_S = 18K's'$ and the K' values of these samples are closely on the universal curve, the deviation of s' from the universal curve to the higher side is mainly correlated with τ_S deviating towards the same side.

As shown in figure 7, being a little beyond the range of error fluctuations from the universal curve, the s' data points of L10 appear to be on the verge of deviating from the universality. When multiplied by a constant, the calculated universal curve can be shifted upwards to superpose well on the s' data points of L10, A5000 and A2500 individually as shown by the dotted lines in figure 7. By extrapolating the thus obtained multiplication factors, it is estimated that deviation from the universal curve begins around $M_w = 12\,000$, which is between the M_w value of L10 and M_e. Thus, although the universal curve is applicable in both entangled (samples A and B) and entanglement-free (sample C) systems, as shown in the last section, the applicable entanglement-free region as revealed here is quite narrow.

It is interesting to compare τ_S results shown in figure 6 with the dielectric-relaxation times τ_{dielec} of polystyrene samples as shown in figure 4 of the paper of Roland and Casalini [56] (R&C). Both sets of results are plotted against $\Delta T = T - T_g$; however, R&C define T_g as corresponding to $\tau_{dielec} = 100$ s as opposed to $\tau_S = 1000$ s being used in this study. The difference in the definition of T_g should matter little if these two sets of results are not to be compared quantitatively. Among the seven samples studied in R&C's paper, five are of very low molecular weight; only two have molecular weights greater than M_e. The τ_{dielec} results of the five low-molecular-weight samples qualitatively show the trend of deviating upward from the results of the two high-molecular-weight samples, which are very close to each other. R&C's results do not show a consistent increase in deviation with decreasing molecular weight; instead, their deviations behave in an erratic way. Despite the erratic behavior, R&C state in their paper 'Although there is significant scatter, the deviations are systematic with molecular weight'. Thus, ignoring the erratic behavior of their data, R&C expect the kind of consistent trend of deviation from the universal curve as presented in figure 6, since the results of their two high-molecular-weight samples appear nearly on top of each other.

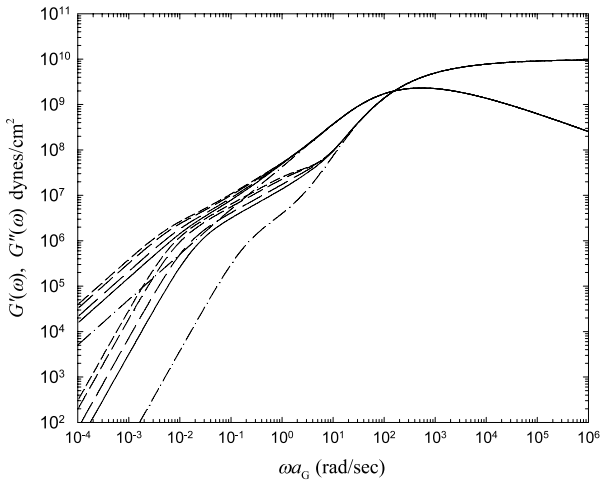

Figure 9. Comparison of the viscoelastic spectra $G^*(\omega)$ of sample C at different temperatures or ΔT calculated from the parameters extracted from the analyses of its $J(t)$ results (—— in the glassy-relaxation region; in the entropic region — · — at $T_g = 93.8\,^\circ$C ($\Delta T = 0$), —— at 108.8 °C ($\Delta T = 15\,^\circ$C), — — — at 113.8 °C ($\Delta T = 20\,^\circ$C), – – – at 123.8 °C ($\Delta T = 30\,^\circ$C) and - - - - at 133.8 °C ($\Delta T = 40\,^\circ$C)); the reference temperature is 108.8 °C.

8.3. Comparison of the $G^*(\omega)$ spectra of sample C and L10

For further illustrating the consistency between the $J(t)$ and $G^*(\omega)$ results, the $G^*(\omega)$ spectra of sample C calculated from the parameters extracted from analyzing its $J(t)$ results are shown in figure 9 for comparison with those of L10 shown in figure 5. In both the figures, spectra at equivalent ΔT values are shown for a one-to-one comparison. As the reference temperature chosen in figure 5 for L10 is equivalent to $\Delta T = 15\,^\circ$C, the spectra shown in figure 9 for sample C are superposed on each other over the glassy-relaxation region with the reference chosen at 108.8 °C ($\Delta T = 15\,^\circ$C). Both L10 and sample C being free of entanglement with some difference in molecular weight, the great similarity between the two sets of spectra at equivalent ΔT values is expected based on what have been shown in figures 6–8. Figure 9 also shows the spectrum of sample C at $\Delta T = 0$ (or at $T_g = 93.8\,^\circ$C); the equivalent information for L10 is unavailable from the data of Inoue *et al* [32]. Both being at the same ΔT, the frequency-scale of the glassy-relaxation region as shown in figure 5 for L10 is about 25% off that shown in figure 9 for sample C. At $\Delta T = 15\,^\circ$C, $\tau_S = 0.089$ s (or $\langle\tau\rangle_G = 4.9 \times 10^{-3}$ s) for L10 as opposed to $\tau_S = 0.069$ s (or $\langle\tau\rangle_G = 3.8 \times 10^{-3}$ s) for sample C, in accord with τ_S of L10 being slightly above the universal curve, as shown in figure 6.

9. Information in the obtained $G(t)$ curves

9.1. Length-scale at T_g

With the s' and K' values determined for samples A, B and C at their individual T_g points in section 8, the $G_p(t)$ curves of the three samples may be calculated using equations (4)–(7) for sample A and sample B and equations (7)–(11) for sample C. The three calculated $G_p(t)$ curves are shown together in figure 10 for a revealing comparison. In the figure, the curves calculated by setting A_G (or A_G^f) $= 0$ are also shown; in each set of curves, the area between the full curve and the curve with A_G (or A_G^f) $= 0$ represents the contribution of the glassy-relaxation process

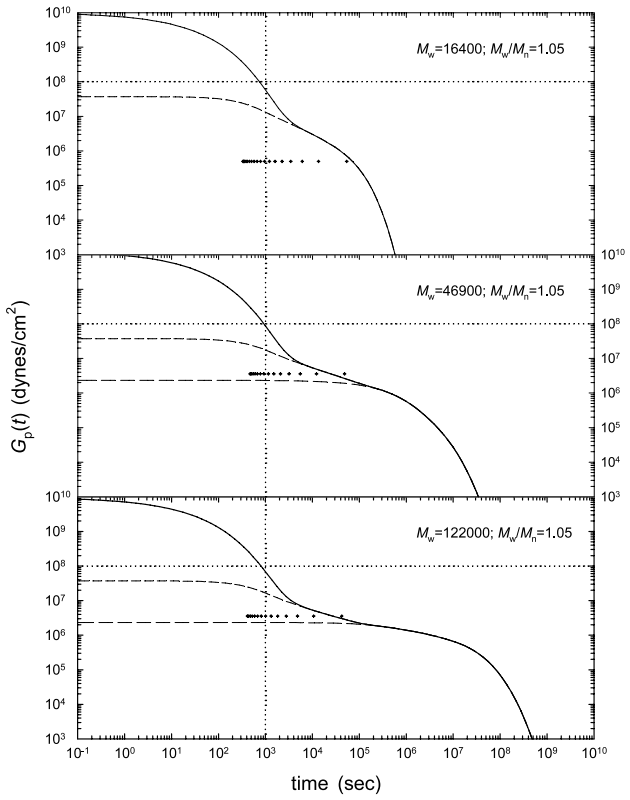

Figure 10. Comparison of the $G_p(t)$ figures of sample A (middle), sample B (bottom) and sample C (top) at individual T_g or $\Delta T = 0$. In each figure, the relaxation times of the Rouse–Money normal modes (for sample A and sample B) or the Rouse normal modes (for sample C) are indicated by +, the line - - - - is calculated with A_G^f or $A_G = 0$ and the line – – – is calculated with $A_G = 0$ as well as setting the contribution of the Rouse–Mooney normal modes to zero. The common vertical dotted line represents the structural-relaxation time $\tau_S = 1000$ s. The points where the $G_p(t)$ curves cross the horizontal dotted lines at 10^8 dyn cm^{-2} represent traditionally defined structural- (or α-) relaxation times.

to the relaxation modulus $G_p(t)$. For sample A and sample B, the curves calculated without both the glassy relaxation and Rouse–Mooney normal modes are also shown; the area between a thus calculated curve and that with $A_G = 0$ represents the contribution of the Rouse–Mooney normal modes to $G_p(t)$. Also indicated in the figure are the positions in time corresponding to the relaxation times of the Rouse normal modes in sample C and the relaxation times of the Rouse–Mooney normal modes in sample A and sample B.

It has been proposed in [4] that the positions of the relaxation times of the normal modes may be used as 'graduations' of an internal yardstick for estimating the extent of influence of the glassy-relaxation process. The relaxation time of the pth normal mode, τ_A^p (in the Rouse–Mooney process of sample A and sample B) or τ_p (in the Rouse process of sample C), is associated with a length-scale given by [2, 57]

$$\lambda_p \approx (a^2/p)^{0.5}, \tag{18}$$

with a standing for the entanglement distance in the entangled case (sample A and sample B) or for the end-to-end distance in the entanglement-free case (sample C). The value a may be calculated from the characteristic ratio C_∞ or equivalently K_∞ (=0.43 ×

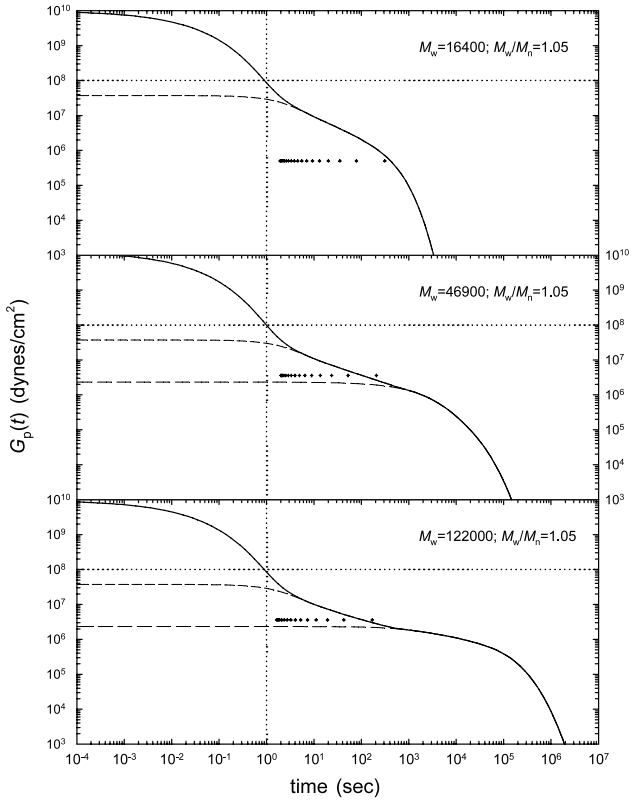

Figure 11. Comparison of the $G_p(t)$ figures of sample A (middle), sample B (bottom) and sample C (top) at $\Delta T = 9.7\,^{\circ}$C. In each figure, the relaxation times of the Rouse–Money normal modes (for sample A and sample B) or the Rouse normal modes (for sample C) are indicated by $+$, the line - - - - is calculated with A_G^f or $A_G = 0$ and the line $---$ is calculated with $A_G = 0$ as well as setting the contribution of the Rouse–Mooney normal modes to zero. The common vertical dotted line represents the structural-relaxation time $\tau_S = 1$ s. The points where the $G_p(t)$ curves cross the horizontal dotted lines at 10^8 dyn cm^{-2} represent traditionally defined structural- (or α-) relaxation times.

10^{-2} nm^2 Da^{-1} for polystyrene) [2, 58, 59]; one obtains $a^2 = K_\infty M_e = 58.1$ nm^2 for sample A and sample B, and $a^2 = K_\infty M_w = 70.5$ nm^2 for sample C. One sees in figure 10 that the vertical dotted line at 10^3 s on the time coordinate, representing the structural-relaxation time τ_S at T_g, passes through between the relaxation times of the seventh and eighth normal modes in all three cases. Using the position of $\tau_S = 10^3$ relative to τ_A^7 and τ_A^8 or to τ_7 and τ_8, we may calculate from the values of λ_7 and λ_8 (equation (18)) the length-scale λ at T_g by interpolation. The λ values so obtained are 2.76, 2.87 and 3.0 nm for samples A, B and C, respectively. These values are consistent with one another; furthermore, they are virtually the same as that estimated by the calorimetric method for polystyrene at T_g [48, 49].

9.2. Change in length-scale with ΔT

According to the calculated curve shown in figure 6, $\tau_S = 1$ s occurs at $\Delta T = 9.7\,^{\circ}$C. For illustrating the change in length-scale with ΔT occurring in samples A, B and C in perspective, shown in figure 11 is the comparison of the $G_p(t)$ curves of the three samples calculated at

$\Delta T = 9.7\,^{\circ}\mathrm{C}$. The parameters s' and K' used to calculate the $G_{\mathrm{p}}(t)$ curve for each of the samples are obtained from the values determined at different temperatures by interpolation through least-squares fittings. As shown in the figure, the vertical dotted line at 1 s representing the structural-relaxation time occurs before the relaxation time of the highest Rouse or Rouse–Mooney mode by about an equal 'distance' in all three cases—equivalent to log 1.9, log 2.0 and log 1.6 for samples C, A and B, respectively. Clearly, the consistency among the three samples as observed at $\Delta T = 0$ (figure 10) is preserved at $\Delta T = 9.7\,^{\circ}\mathrm{C}$. $\tau_{\mathrm{S}} = 1$ s being shorter than the motional time of a single Rouse segment means that the length-scale associated with the structural-relaxation process is shorter than the Rouse-segmental length of ∼2 nm, indicating a rubbery state. By contrast, the length-scale reaches ∼3 nm at $\Delta T = 0$ (figure 10), indicating vitrification at the Rouse-segmental level.

10. Discussion

10.1. Frictional slowdown and structural growth

As proposed previously [2, 9, 11, 38] and supported by the universal ΔT dependence of K' shown in figure 8, the molecular-weight dependence of K' and that of T_{g} are directly related to each other. The consistency of the ΔT dependence of s' among the three samples indicates that the molecular-weight dependence of K' extends into the time domain of the glassy-relaxation process as indicated by equation (15). In other words, after the T_{g} correction is made to both the $\mu_{\mathrm{A}}(t)$ (or $\mu_{\mathrm{R}}(t)$) and $\mu_{\mathrm{G}}(t)$ processes by expressing K' and s' in terms of ΔT, all of them become independent of molecular weight. This also means that the molecular-weight dependence of T_{g} in the entanglement region is directly related to the fast dynamic processes, $\mu_{\mathrm{A}}(t)$ and $\mu_{\mathrm{G}}(t)$, both following the same molecular-weight dependence.

While K' is a frictional factor, s' having the unit of Da^2 is a structural factor [4]. Thus the ΔT dependence of s' (figure 7) and that of K' (figure 8) are of different physical natures. With decreasing ΔT, the former represents the growth of some T_{g}-related structure while the latter represents purely the frictional slowdown of the Rouse segment. The structural relaxation (i.e. $\mu_{\mathrm{G}}(t)$) with relaxation time defined by equation (15) contains the effects of both the frictional slowdown and structural growth while the $\mu_{\mathrm{A}}(t)$ or $\mu_{\mathrm{R}}(t)$ process is only affected by the frictional slowdown. As a result, the positions of τ_{S} relative to $\{\tau_{\mathrm{A}}^{p}\}$ or $\{\tau_{p}\}$ in timescale change with ΔT as observed in the comparison of figures 10 and 11.

10.2. K values in the close neighborhood of T_{g}

As shown in figures 10 and 11, all three samples have length-scales of the same magnitude at $\tau_{\mathrm{S}} = 1000$ or 1 s (at $\Delta T = 0$ or $9.7\,^{\circ}\mathrm{C}$). These revealed uniformities result directly from the universal behavior of s' and K' as a function of ΔT. As figures 10 and 11 are all displayed in real time, the shown positions of the relaxation times are ultimately determined by the K values. As the temperature is approaching T_{g} ($\Delta T \lesssim 20$; in this temperature region $\tau_{\mathrm{S}} \gtrsim 1^{-2}$ s), because $K' = K R_K (M/M_{\mathrm{e}})$ ($K' = 1.61K$ for sample A; $K' = 3.16K$ for sample B; and $K' = K$ for sample C) K has to change with ΔT in such a way that the corresponding K' values will behave in the universal way as shown in figure 8. As the temperature approaches near T_{g}, with this effect becoming important, K has to become influenced by the position of T_{g}, which declines with decreasing molecular weight below $\sim 10 M_{\mathrm{e}}$ for polystyrene [38, 39]. This has to be reconciled with the fact that K is independent of molecular weight at and above $127.5\,^{\circ}\mathrm{C}$ (see footnote 4). As shown in figure 12 and explained in the following, the comparison of the K values as a function of temperature between samples A, B and C illustrates such a transition.

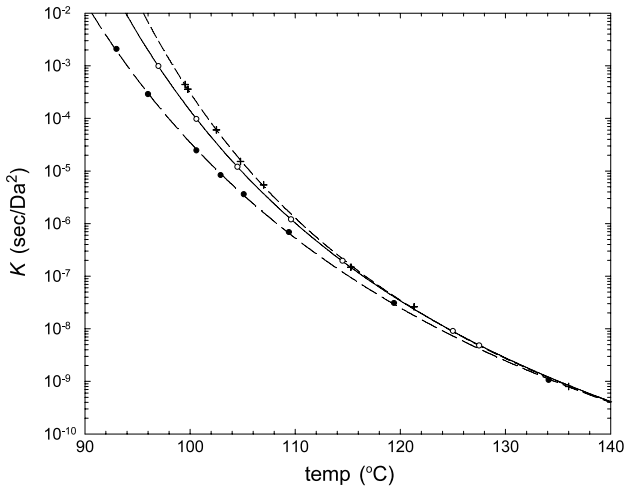

Figure 12. The comparison of K values as a function of temperature between sample A (○), sample C (●) and the hypothetically uncontaminated sample B (+) (see the text). The lines are calculated from the FTH equations best fitting the experimental data: —— for sample A, – – – for sample C and - - - - for the hypothetically uncontaminated sample B.

Sample C and F1 have nearly the same M_w values and virtually the same K value (table 1). As described by the Rouse theory, the viscoelastic response of sample C has only one frictional factor K—isotropic dynamically. In the case of F1, because its molecular weight is so close to M_e, $K = K'$ within a small experimental error—virtually isotropic dynamically. Thus, the difference in the physical meaning of K between sample C and F1 should be very small. Based on these obtained results, the K values of sample C and F1 as a function of temperature should be very close to each other. The pattern that the K values of sample A and sample C diverge as the temperature approaches T_g and merge at high temperatures, $\gtrsim$130 °C, as shown in figure 12, should similarly occur between sample A and F1. At 127.5 °C the K values (table 1) for sample C and F1 are about 17–20% smaller than the average value $K = 4.9 \times 10^{-9} \pm 10\%$ as obtained over the molecular weight range from 3.4×10^4 to 6.0×10^5 (table 1 and appendix B of [4]) [2, 4, 9]. The 17–20% smaller K for sample C and F1 is mostly likely due to the effect of a substantially smaller T_g (by ∼6 °C). In any case, as these differences in K are so small, these results actually confirm that the ERT and the Rouse theory have the same footing at the Rouse-segmental level.

Because sample B is contaminated by residual plasticizers [7], the K values of sample B cannot be directly compared with those of sample A [4]. To illustrate the point made above, the curve calculated from the FTH equation that has been obtained from the least-squares fitting to the K values of sample B is shifted to the higher-temperature side by 1.5° in figure 12. The temperature shift is to account for the decrease in T_g caused by the contamination of residual plasticizers. The magnitude of the shift is chosen such that after the shift the curve superposes closely on the FTH curve of sample A over the region above 118 °C. The shift is of the magnitude estimated by Plazek [7]. The close superposition automatically includes the expectation that the K value of the 'uncontaminated sample B' be in close agreement with that of sample A at 127.5 °C. After such a shift, the FTH curve of sample B begins to rise above that of sample A below ∼115 °C, illustrating divergence similar to that between sample A and sample C, but in a smaller degree. If we use the universal value $K' = 1.35 \times 10^{-3}$ expected at $\Delta T = 0$ (see figure 8), the K value at T_g for the 'uncontaminated sample B' should be

4.27×10^{-4} ($=K'/3.16$), which occurs at 99.55 °C on the shifted FTH curve of sample B. This T_g value is consistent with the sum of the shift (1.5°) and the T_g value of sample B (98.03 °C) determined by $\tau_S = 1000$ s. Thus, we have the T_g values for sample A, uncontaminated sample B and sample C as 97, 99.55 and 93.8 °C, respectively; these values are consistent with what may be expected from calorimetric measurements (see table 1).

10.3. Effect of chain connectivity

Values of τ_S, s' and K' obtained for L10 cling closely to the respective universal curves established on the results of sample A, sample B and sample C. The low end of the molecular weight range covered by these samples is higher than that of L10 by about 6000. The small deviations of L10's results from the universal curves are in the directions expected from the larger deviations observed in the other samples of even smaller molecular weights. In other words, the small deviations of L10 must be caused by the effects that will set in when the molecular weight is sufficiently low. One important factor may be the reduction in the hindrance to segmental movement as chain connectivity is sufficiently reduced, as supported by the following analysis. Figure 8 shows that K' being the same at a fixed ΔT is true down to molecular weights as low as A5000, and nearly so for A2500. With K' remaining the same, in the same way as equation 10 of [4] has been obtained, the following relationship—a physical constraint—can be obtained:

$$\frac{d^2}{s'} = \text{const}, \tag{19}$$

where d represents the average distance the Rouse segment jumps in one step. As the hindrance to segmental movement is reduced with decreasing molecular weight, a larger jumping-step length d may be allowed; then based on equation (19) s' becomes larger. This explains the further shift of s' from the universal curve to the higher side—at a fixed ΔT—as molecular weight decreases as shown in figure 7.

11. Summary

The ultimate goal of this report is to bring together the results of entangled systems studied previously [4, 5] and of the presently studied entanglement-free systems, and present the analysis-obtained results pertinent to the T_g-related thermorheological complexity. The analyses done in and the results obtained from both the studies are jointly summarized for giving a comprehensive view.

The quantitative success of the extended reptation theory (ERT; for entangled systems) [2, 8–11] and the Rouse theory (for entanglement-free systems) [2, 10, 15, 16, 35] in describing the polymer relaxation modulus $G(t)$ or viscoelastic spectrum $G^*(\omega)$ over the entropic region allows them to be used as the frame of reference. The $G(t)$ functional forms covering the whole time range are given by incorporating a stretched exponential for the glassy-relaxation process $\mu_G(t)$ into the ERT or the Rouse theory. The creep compliance $J(t)$ curves of entangled (sample A and sample B) [6, 7] and entanglement-free (sample C) [31] polystyrene samples as well as the viscoelastic spectra $G^*(\omega)$ of entanglement-free polystyrene samples (L10, A5000, A2500 and A1000) [32] have been quantitatively analyzed in terms of the given $G(t)$ functional forms.

From the $J(t)$ line-shape analyses, the structural-relaxation time $\tau_S = 18\langle\tau\rangle_G$ ($\langle\tau\rangle_G$ being the average glassy-relaxation time), the structural-growth parameter s' and the frictional factor K' for the Rouse–Mooney process $\mu_A(t)$ or the Rouse process $\mu_R(t)$ are extracted. Representing a very significant aspect of the analyses, the separation of $\tau_S(= 18s'K')$ into

the two decoupled quantities s' and K' is a fundamentally clean-cut process: while s' is determined entirely by the *line shape* of $J(t)$ or $G^*(\omega)$, K' is determined by the timescale *shifting factor* obtained from superposing the calculated $J(t)$ or $G^*(\omega)$ on the measured one. Very significantly, the uneven temperature dependences in different time regions of $J(t)$ for sample A, sample B and sample C are described in a natural and precise way by a simple increase in the structural-growth parameter s' with decreasing temperature. In the case of sample C, the decline in the steady-state compliance J_e^0 with temperature decreasing towards the glass transition point T_g is simultaneously so described quantitatively.

For all the studied samples, T_g is defined by the temperature at which the structural-relaxation time $\tau_S = 1000$ s. When the dynamic and structural quantities τ_S, s' and K' of samples A, B and C are displayed as a function of $\Delta T = T - T_g$, they fall individually on the same curves. Bases are pointed out for claiming that the common curves shared by the three samples represent a T_g-related universality within the polystyrene system, entangled or not. As the ERT and the Rouse theory are independently involved, the established universality also confirms the conclusion from the study of the blend-solution systems [2, 11] that the ERT and the Rouse theory have the same footing at the Rouse-segmental level. Because of the universal dependence of s' and K' on ΔT, the $\mu_G(t)$ process and the $\mu_A(t)$ or $\mu_R(t)$ process in both their absolute and relative positions in time depend on ΔT in the same way.

In addition, the importance of the role of the Rouse segment as a reference in both timescale and length-scale is revealed. The relaxation times of the Rouse–Mooney normal modes (for sample A and sample B) or the Rouse normal modes (for sample C) have been used as the 'graduations' of an internal yardstick for estimating the extent of influence of the glassy relaxation near and at T_g. As a logical consequence of s' and K' depending on ΔT in a universal way, the length-scales increase gradually in the same way and reach ∼3 nm at $\Delta T = 0$ (or at T_g) for the three samples covered by the universality.

The τ_S, s' and K' results obtained from analyzing the $G^*(\omega)$ spectra of samples with molecular weights just below and well below the entanglement molecular weight $M_e = 13\,500$ (L10, A5000, A2500 and A1000) are compared with those of samples A, B and C. The comparison reveals that deviation from the universality established on the analysis-obtained results of sample A, B and C increases with decreasing molecular weight. Deviation is estimated to begin around $M_w = 12\,000$, which is only 10% below M_e and about 30% below the M_w of sample C—sample C with $M_w = 16\,400 > M_e$ becomes an entanglement-free system because its molecular-weight distribution is not extremely narrow. Thus, although the universality is applicable in both the entangled and entanglement-free polystyrene systems, the applicable entanglement-free region is quite narrow.

Acknowledgments

This work is supported by the National Science Council (NSC 93-2113-M-009-015, NSC94-2113-M-009-002). The author thanks Dr T Inoue for supplying the $G^*(\omega)$ data of L10, A5000, A2500 and A1000 published in [32].

Appendix A. $G^*(\omega)$ spectra of A5000, A2500 and A1000

Shown in figure A.1 are the composite $G^*(\omega)$ spectra of A5000, A2500 and A1000 formed and analyzed as described in section 4.

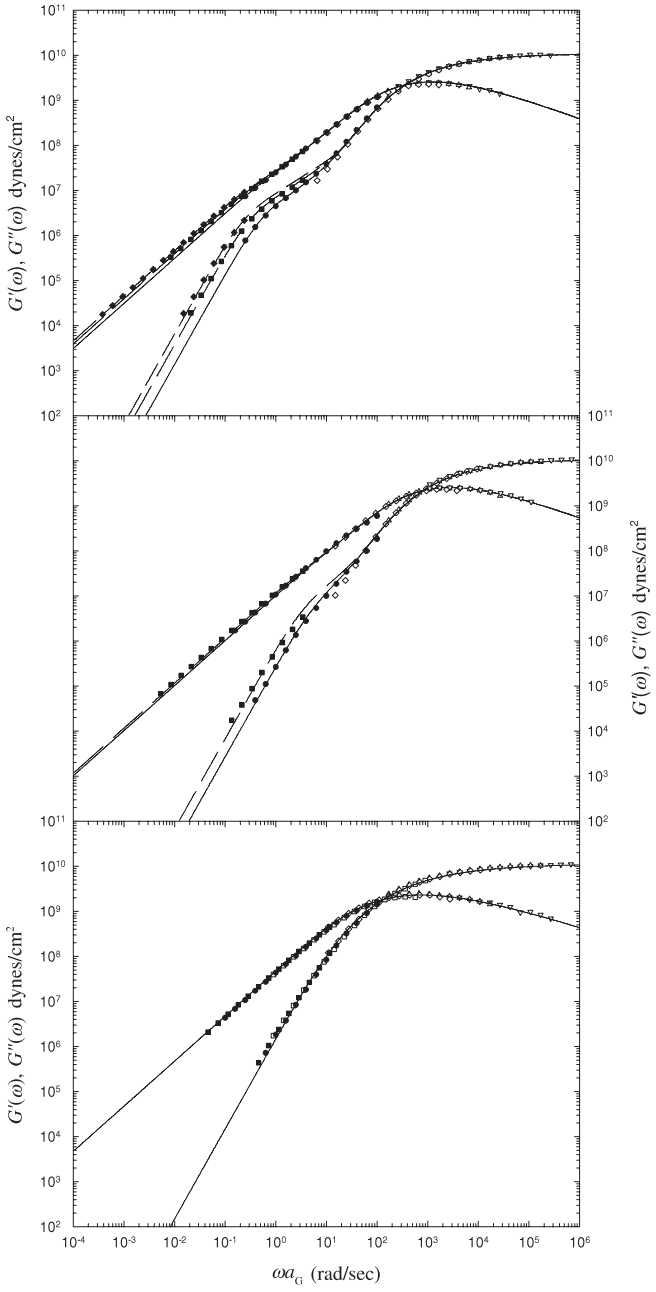

Figure A.1. Top: comparison of the viscoelastic spectra $G^*(\omega)$ of A5000 measured at different temperatures (▽ at 85 °C; △ at 88 °C; ◇ at 92 °C; ● at 100 °C; ■ at 110 °C; ♦ at 120 °C) with the calculated (—— in the glassy-relaxation region; in the entropic region —— at 100 °C, — — — at 110 °C and – – – at 120 °C); the reference temperature is 100 °C. Middle: comparison of the viscoelastic spectra $G^*(\omega)$ of A2500 measured at different temperatures (▽ at 62 °C; △ at 65 °C; ◇ at 70 °C; ● at 80 °C; ■ at 90 °C) with the calculated (—— in the glassy-relaxation region; in the entropic region —— at 80 °C and — — — at 90 °C); the reference temperature is 80 °C. Bottom: comparison of the viscoelastic spectra $G^*(\omega)$ of A1000 measured at different temperatures (▽ at 5 °C; △ at 10 °C; ◇ at 15 °C; □ at 20 °C; ● at 25 °C; ■ at 30 °C) with the calculated one (——); the reference temperature is 25 °C.

Appendix B. T_g values of L10, A5000, A2500 and A1000 determined at $\tau_S = 1000$ s

For showing the τ_S results of L10, A5000, A2500 and A1000 as a function of ΔT in figure 6, their glass-transition temperatures T_g, defined as the point where $\tau_S = 1000$ s, need to be determined individually first. As the longest τ_S values extracted from the data of Inoue *et al* [32], except for A1000, are around 100–200 s, the T_g values cannot be determined by interpolation. Under the circumstance, one may do two things: one is by doing extrapolation based on the FTH equation that best fits the available data; the other is by superposing the longest τ_S data point onto the curve calculated from equation (16) by shifting along the ΔT coordinate. The T_g values determined in these two ways differ by less than 0.3°; either way does not lead to a difference in interpretation. The $T_g(\tau_S = 1000\ \text{s})$ values listed in table 1 and used in calculating ΔT for plotting the τ_S points in figure 6 are the results of using extrapolation based on the FTH equation. As shown in table 1, these T_g values are consistent with the values determined by DSC as closely as those of sample A, sample B and sample C are. In the case of A1000, the temperature dependence of the τ_S results are fitted to the FTH equation, from which the T_g point where $\tau_S = 1000$ s is determined by interpolation.

References

[1] Ferry J D 1980 *Viscoelastic Properties of Polymers* 3rd edn (New York: Wiley)
[2] Lin Y-H 2003 *Polymer Viscoelasticity: Basics, Molecular Theories, and Experiments* (Singapore: World Scientific)
[3] Tschoegl N W 1989 *The Phenomenological Theory of Linear Viscoelastic Behavior* (Berlin: Springer)
[4] Lin Y-H 2005 *J. Phys. Chem.* B **109** 17654
[5] Lin Y-H 2005 *J. Phys. Chem.* B **109** 17670
[6] Plazek D J 1965 *J. Phys. Chem.* **69** 3480
[7] Plazek D J 1968 *J. Polym. Sci.* A2 **6** 621
[8] Lin Y-H 1984 *Macromolecules* **17** 2846
[9] Lin Y-H 1986 *Macromolecules* **19** 159
[10] Lin Y-H 1986 *Macromolecules* **19** 168
[11] Lin Y-H 1987 *Macromolecules* **20** 885
[12] Lin Y-H 1989 *Macromolecules* **22** 3075
[13] Lin Y-H 1989 *Macromolecules* **22** 3080
[14] Lin Y-H 1991 *Macromolecules* **24** 5346
[15] Rouse P E Jr 1953 *J. Chem. Phys.* **21** 1271
[16] Bird R B, Curtiss C F, Armstrong R C and Hassager O 1987 *Dynamics of Polymeric Liquids* vol 2 *Kinetic Theory* 2nd edn (New York: Wiley)
[17] Hopkins I L and Hamming R W 1957 *J. Appl. Phys.* **28** 906
[18] Hopkins I L and Hamming R W 1958 *J. Appl. Phys.* **29** 742
[19] Fulcher G S 1925 *J. Am. Chem. Soc.* **8** 339
Fulcher G S 1925 *J. Am. Chem. Soc.* **8** 789
[20] Tammann G and Hesse G 1926 *Z. Anorg. Allg. Chem.* **156** 245
[21] Williams M L, Landel R F and Ferry J D 1955 *J. Am. Chem. Soc.* **77** 3701
[22] Inoue T, Okamoto H and Osaki K 1991 *Macromolecules* **24** 5670
[23] Inoue T, Hayashihara H, Okamoto H and Osaki K 1992 *J. Polym. Sci. Polym. Phys. Edn* **30** 409
[24] Inoue T and Osaki K 1996 *Macromolecules* **29** 1595
[25] Inoue T, Uematsu T and Osaki K 2002 *Macromolecules* **35** 820
[26] Lin Y-H 1994 *J. Polym. Res.* **1** 51
[27] Lin Y-H and Lai C S 1996 *Macromolecules* **29** 5200
[28] Lai C S, Juang J-H and Lin Y-H 1999 *J. Chem. Phys.* **110** 9310
[29] Lin Y-H and Luo Z-H 2000 *J. Chem. Phys.* **112** 7219
[30] Lin Y-H 2002 *J. Chin. Chem. Soc.* **49** 629
[31] Plazek D J and O'Rourke V M 1971 *J. Polym. Sci.* A2 **9** 209
[32] Inoue T, Onogi T, Yao M-L and Osaki K 1999 *J. Polym. Sci.* B **37** 389
[33] Mooney M 1959 *J. Polym. Sci.* **34** 599

[34] Doi M 1980 *J. Polym. Sci. Polym. Phys. Edn* **18** 1005
[35] Lin Y-H and Juang J-H 1999 *Macromolecules* **32** 181
[36] Schulz G V Z 1943 *Phys. Chem. Abst.* B **43** 25
[37] Tung L H 1967 *Polymer Fractionation* ed M J R Cantow (New York: Academic)
[38] Lin Y-H 1990 *Macromolecules* **23** 5292
[39] Rudin A and Burgin D 1975 *Polymer* **16** 291
[40] Doolittle A K 1951 *J. Appl. Phys.* **22** 1471
[41] Doolittle A K 1952 *J. Appl. Phys.* **23** 236
[42] Doolittle A K 1952 *J. Appl. Phys.* **23** 418
[43] Cohen M H and Turnbull D 1959 *J. Chem. Phys.* **31** 1164
[44] Turnbull D and Cohen M H 1961 *J. Chem. Phys.* **34** 120
[45] Berry G C and Fox T G 1968 *Adv. Polym. Sci.* **5** 261 and references therein
[46] Doi M and Edwards S F 1978 *J. Chem. Soc. Faraday Trans.* 2 **74** 1789
[47] Doi M and Edwards S F 1978 *J. Chem. Soc. Faraday Trans.* 2 **74** 1802
[48] Sillescu H 1999 *J. Non-Cryst. Solids* **243** 81 and references therein
[49] Hempel E, Hempel G, Hensei A, Schick C and Donth E 2000 *J. Phys. Chem.* B **104** 2460
[50] Tracht U, Wilhelm M, Heuer A, Feng H, Schmidt-Rohr K and Spiess H W 1998 *Phys. Rev. Lett.* **81** 2727
[51] Cicerone M T, Blackburn F R and Ediger M D 1995 *J. Chem. Phys.* **102** 471
[52] Arndt M, Stannarius R, Groothues E, Hempel E and Kremer F 1997 *Phys. Rev. Lett.* **79** 2077
[53] Angell C A 1995 *Science* **267** 1924 and references therein
[54] Angell C A 1991 *J. Non-Cryst. Solids* **131–133** 13
[55] Binder K and Kob W 2005 *Glassy Materials and Disordered Solids* (Singapore: World Scientific)
[56] Roland C M and Casalini R 2003 *J. Chem. Phys.* **119** 1838
[57] Doi M and Edwards S F 1986 *The Theory of Polymer Dynamics* (New York: Oxford University Press)
[58] Lin Y-H 1987 *Macromolecules* **20** 3080
[59] Fetters L J, Lohse D J, Richter D, Witten T A and Zirkel A 1994 *Macromolecules* **27** 4639